Multimedia Tools and Applications (2021) 80:21843–21883
https://doi.org/10.1007/s11042-021-10672-y

Multiply distorted image quality assessment based on feature level fusion and optimal feature selection

Imran Fareed Nizami[1] · Mehreen Akhtar[2] · Asad Waqar[1] · Amer Bilal Mann[3] · Muhammad Majid[2]

Received: 3 July 2020 / Revised: 1 October 2020 / Accepted: 4 February 2021 /
Published online: 20 March 2021

Abstract

No reference image quality assessment (NR-IQA) has received considerable importance in the last decade due to a rise in the use of multimedia content in our daily lives. Due to limitations in technology, multiple distortions may be introduced in the images that need to be assessed. Recently feature selection has shown promising results for single distorted NR-IQA and their effectiveness on multiple distorted images still need to be addressed. In this paper, impact of feature level fusion and feature selection on multiple distorted image quality assessment is presented. To this end features are extracted from multiple distorted images using six NR-IQA techniques (BLIINDS-II, BRISQUE, CurveletQA, DIIVINE, GM-LOG, SSEQ) that extract features in different (discrete cosine transform, spatial, curvelet transform, wavelet transform, spatial and gradient, spatial and spectral) domains. The extracted features from different domains are fused to generate a single feature vector. All combinations of feature-level fusion from six different techniques have been evaluated. Three different feature selection algorithms (genetic search, linear forward search, particle swarm optimization) are then applied to select optimum features for NR-IQA. The selected features are then used by the support vector regression model to predict the quality score. The performance of the proposed methodology is evaluated for two multiple distorted IQA databases (LIVE multiple distorted image dataset (LIVEMD), multiply distorted image database (MDID2017)), two singly synthetically distorted IQA databases (Tampere image database (TID2013), Computational and subjective image quality database (CSIQ)), and one screen content IQA database (Screen content image quality database (SIQAD)). Experimental results show that the fusion of features from different domains gives better performance in comparison to existing multiple-distorted NR-IQA techniques with SROCC scores of 0.9555, 0.9587, 0.6892, 0.9452, and 0.7682 on the LIVEMD, MDID, TID2013, CSIQ, and SIQAD databases respectively. Moreover, the performance is further improved when the genetic search feature selection algorithm is applied to fused features to remove the redundant and irrelevant features. The SROCC scores are improved to 0.9691, 0.9723, and 0.6897 for LIVEMD, MDID, and TID2013 databases respectively.

✉ Imran Fareed Nizami
imnizami.buic@bahria.edu.pk

Extended author information available on the last page of the article.

Keywords No reference image quality assessment · Multiply distorted images · Feature selection · Feature extraction · Feature level fusion

1 Introduction

Nowadays a large number of images are shared over the internet every day, which are captured using digital cameras and transmitted over wireless networks. The quality of images is important in many imaging applications. Distortion may be introduced in images during acquisition, storage, or transmission due to limitations in technology. Contrast and blur type distortion is introduced in images during image acquisition. Blockiness, blur, and ringing distortion type is introduced by image compression and coding techniques. All these factors contribute to degrading the quality of images received by the end-user.

Image quality assessment (IQA) performed by humans is known as subjective IQA and it is deemed to be the standard. Subjective IQA suffers from many disadvantages that include the requirement of a large amount of time, the tedious nature of the task, and the effect of the evaluators' mood on the quality score. Therefore, developing computational models that can predict the quality of images, which correlates with human perception has gained importance. These computational models are based on objective metrics and are known as Objective IQA.

Objective IQA is further categorized into full reference (FR), no-reference approach (NR), and reduced reference approach (RR) IQA techniques. FR and RR-IQA techniques are limited in their usability because the whole reference image or features extracted from the reference image are required, which may not be available in real-world scenarios [14, 39, 58]. NR-IQA techniques offer the advantage of not requiring the reference image, therefore they can be easily used in real-world scenarios. Many NR-IQA techniques are designed for images affected by single distortion types and significant achievements have been made in IQA. However, in practical scenarios images are usually distorted by more than one distortion type. One approach to IQA in images with multiple distortions is to determine the individual distortion type and then compute the quality score due to each distortion type and then determine the overall quality score [33]. However, these types of techniques require prior knowledge about the distortion types affecting the image, which is usually not available and does not take into consideration the joint effects of the multiple distortions.

In [51], improved multiscale local binary pattern (IMLBP) is used to assess the quality of images affected by multiple distortions. The IMLBP consists of the local binary pattern (LBP) and the radius diffference LBP, where the radius difference LBP measures changes in the radial direction. Multiply distorted images are decomposed over multiple scales using Gabor transform, and its phase congruency, phase congruency covariance maxima, phase congruency covariance minima, contrast sensitivity, and gray level-gradient co-occurrence matrix to assess the quality of images [20]. A unified model for singly and multiply distorted stereoscopic images is proposed in [13], which jointly minimizes reconstruction error, quality inconsistency in a supervised dictionary-based learning model to assess the quality of images. In [56], a three-layer classification model is utilized to identify 19 distortion types and 14 contrast features are employed with a multilayer probability-weighting rule in a most-apparent-distortion strategy to adaptively combine five quality scores based on outputs of three classification models to assess the quality of single and multiply distorted images. Phase congruency and LBP are used to model the disruption in intensity values and

distribution of low-level image features, which are used to assess the image quality in multiply distorted images [25]. A FR-IQA method for multiply distorted images based on the local similarity of phase and magnitude of each subband of quaternion wavelet transform is utilized in [19] for predicting the quality score of a multiply distorted images. In [9], structural information of multiply distorted images is extracted using a gradient-magnitude map and contrast-normalized map along with reducing redundancy of features with a random subspace method for predicting the quality of images.

NR-IQA has applications in fire recognition systems as in [5], in which we can assess the quality of images that are being used for fire recognition. NR-IQA can be applied to the results of image segmentation such as in [7] to assess the results of segmentation algorithms. NR-IQA can help in improving the results of object tracking in images by assessing the perceptual quality of images being used in techniques such as in [2, 3]. Saliency detection in image regions such as in [8] can help improve the results of NR-IQA approaches. NR-IQA techniques can help in assessing the performance of inpainting algorithms such as the one given in [6]. The regression models used in NR-IQA can greatly benefit from the incremental and decremental algorithm in [4], since incremental training of the SVR model, can help in reducing training time. Recently, hyperspectral and super-resolution images have gained importance due to their applications in daily life and advancements in technology [1, 40] therefore, NR-IQA of hyperspectral and superresolution images is of interest to researchers. NR-IQA can help by assessing the interface debonding the performance of materials using images and assessing their quality [48]. The quality of images sent by a 5D hyperchaotic four-wing memristive system can be assessed using NR-IQA techniques [49]. One way of evaluating the algorithms with hidden or encrypted data in the images is using NR-IQA techniques so that the perceptual quality before and after data hiding can be assessed [21, 24]. The performance of image blind restoration algorithms can be performed using NR-IQA [57]. Regression models play a vital role in NR-IQA and recently a novel activation function has been proposed for time-variant nonlinear equation [50]. In future works, this kind of activation function can be incorporated to assess the performance of the NR-IQA problem.

All of the aforementioned multiple-distorted NR-IQA techniques extract features from one domain and predict the quality score. As images are affected by multiple distortions, therefore a fusion of features from different domains can improve the performance. Recently, feature selection algorithms have been used in NR-IQA techniques and have shown improvement in existing NR-IQA techniques over images distorted by a single distortion [31, 32, 34]. Feature selection algorithms select optimum features from one domain relevant to the NR-IQA technique to assess the quality of singly distorted images. The proposed methodology in this work is different from existing multiple-distorted and feature selection based methodologies for NR-IQA. In the proposed method, we extract features from existing NR-IQA techniques from different domains and fuse these features for different combinations. Feature selection is then applied to the fused features to select the most relevant features to predict the quality score of multiply distorted images. The major contributions of this work are four-fold,

- A unified methodology is proposed for NR-IQA of singly, multiply distorted, and screen content images that do not require to determine the distortion type affecting the image for assessing the quality of images.
- The impact of feature-level fusion on the quality score prediction for multi-distorted images is analyzed by extracting features from different domains i.e., spatial, DCT, wavelet, curvelet, and spectral domains.

Table 1 Details of different NR-IQA techniques used for evaluation of proposed methodology

NR-IQA technique	Feature domain transform
BLIINDS-II [36]	DCT
BRISQUE [28]	Spatial
CurveletQA [22]	Curvelet and spatial
DIIVINE [30]	Wavelet
SSEQ [23]	Spatial and Spectral
GM-LOG [44]	Spatial

– The impact of feature selection algorithms to remove redundant and irrelevant features to improve the performance of NR-IQA techniques for multiple-distorted images is studied.
– Selection of features extracted in different domain that do not disrupt the NR-IQA process is performed.

The rest of the paper is organized as follows. Section 2 discusses the proposed methodology. Section 3 presents the experimental results on two commonly used subjective IQA databases for multiply distorted images followed by the conclusion in Section 4.

2 Proposed methodology

The objective of this work is to assess the quality of images affected by multiple distortions. Six NR-IQA techniques are used that extract features in different domains. The domain of feature extraction for each NR-IQA is shown in Table 1. The extracted features are used as input to feature selection algorithms to obtain optimum features. The advantage of using feature selection algorithms is to remove redundant features or features that do not contribute to the performance. The selected features are fused using different combinations. Lastly, the features are given as input to a support vector regression model to predict the image quality score. The proposed methodology is shown in Fig. 1.

2.1 Feature extraction

Features extraction is performed using six NR-IQA techniques i.e., Blind Image Integrity Notator using DCT-Statistics (BLIINDS-II), Distortion Identification-based Image Verity and INtegrity Evaluation (DIIVINE), Blind/ Referenceless Image Spatial QUality Evaluator (BRISQUE), Curvelet Quality Assessment (CQA), Spatial Spectral Entropy based

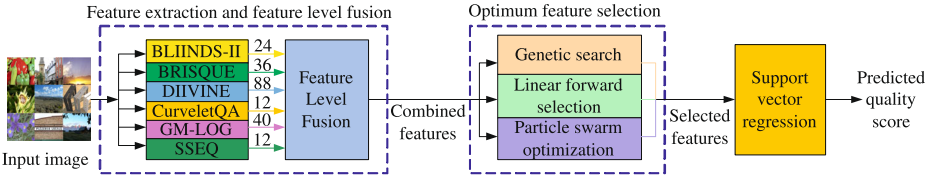

Fig. 1 Proposed methodology for NR-IQA of multiply distorted images using feature level fusion and feature selection

Quality (SSEQ) and Gradient Magnitude Laplacian of Gaussian (GM-LOG). The NR-IQA techniques are selected based on the domain in which features are extracted i.e., BLIINDS-II [36] extracts features in DCT domain, BRISQUE [28] extracts features in the spatial domain, CurveletQA [22] extracts features in Curvelet and spatial domains, DIIVINE [30] extracts features in Wavelet domain, SSEQ [23] extracts features in the spatial and spectral domain, GM-LOG [44] extracts features in the spatial domain, The details of each NR-IQA technique are given below.

2.1.1 Blind image integrity notator using DCT-statistics (BLIINDS-II)

BLIINDS-II is a NR-IQA technique based on a natural scene statistics of discrete cosine transform (DCT) coefficients [36], which are used to predict the image quality score. BLIINDS-II extracts 24 features over three scales using generalized Gaussian model shape parameter, coefficient of frequency variation, energy subband ratio measure, orientation model-based features and uses a simple probabilistic model for image quality score prediction.

2.1.2 Distortion identification-based image verity and integrity evaluation (DIIVINE)

DIIVINE is based on the natural scene statistics (NSS) model which uses a two-step approach for NR-IQA [30]. In the first step, it determines the distortion type present in the image and then uses a distortion specific regression model to predict the image quality. DIIVINE performs normalization on wavelet coefficients to extract statistical characteristics of wavelet coefficients to compute scale and orientation-based statistics, and correlation across scales and spatial correlation. Finally, these statistical features are used with an SVR model to assess the quality of the image.

2.1.3 Blind/reference-less image spatial quality evaluator (BRISQUE)

BRISQUE based on the NSS model, is a blind/no-reference, distortion-generic quality evaluator model which extracts features in the spatial domain [28]. It does not measure specific distortion parameters (e.g. blur, ringing effect, noise, etc.) but it utilizes scene statistics of locally normalized luminance coefficients to measure 'un-naturalness' phenomena from the image using a distance parameter to compute the image quality.

2.1.4 Curvelet quality assessment (CQA)

CurveletQA uses the multiresolution properties of image and orientation statistics in the curvelet domain for NR-IQA [22]. It extracts three groups of features namely asymmetric Gaussian distribution, mean value, kurtosis, and standard deviation of non-cardinal orientation energies, the difference between logarithmic magnitude mean values. SVR is used to predict the image quality score.

2.1.5 Gradient magnitude laplacian of gaussian (GM-LOG)

GM-LOG assesses the quality of distorted images using characteristics of gradient magnitude and Laplacian of Gaussian in a joint adaptive normalization framework [44]. The technique extracts 40 features to determine the type of distortion and then asses the image quality score using a SVR model.

2.1.6 Spatial–spectral entropy-based quality (SSEQ)

SSEQ extracts the features in spatial and spectral domains for assessment of image quality [23]. Entropy is used to measure the information in an image. I was observed that there is a close link between image entropy, the histogram, and image moments. The image is divided into patches of 8×8, spatial and spectral entropy is computed over each image. 12 features are extracted for determining the image quality score. The extracted features are used with SVR to predict the image quality.

2.2 Feature fusion

Once features are extracted using NR-IQA techniques, feature fusion is performed over features of different NR-IQA techniques. All the combinations for feature fusion are analyzed i.e., feature fusion using features of two NR-IQA techniques at one time yields 15 combinations. When feature fusion is performed using features from three NR-IQA techniques at one time, 20 combinations are obtained. Considering features from four NR-IQA techniques at one time yields 15 combinations. Similarly, when features from five NR-IQA techniques are considered at a time 6 combinations are obtained. Lastly, considering features from all the six NR-IQA techniques yields 1 combination. Once features are extracted and feature fusion is performed, then the next step is to perform feature selection.

2.3 Feature selection algorithms

After feature extraction and feature level fusion are performed, the feature vector may contain redundant and irrelevant features for NR-IQA. Feature selection can help in discarding redundant and irrelevant features while retaining the most relevant features, which can help in improving the performance of NR-IQA techniques. Three existing feature selection algorithms have been used to select the most relevant features for NR-IQA. Details of each feature selection algorithm are given below.

2.3.1 Particle swarm optimization (PSO)

PSO feature selection algorithm is based on the environmental behavior of living organs [15]. PSO performs non-linear optimization effectively. Each, 'particle' contains a random solution for the population. Each particle behaves as a D-dimensional space with a fitness value and velocity. The representation of j^{th} particle in population is as $X_j = \{x_{j1}, x_{j2}, x_{j3}, ..., x_{jD}\}$. 'Pre-good' denotes the previous best fitness values of a particle as $f_j = \{f_{j1}, f_{j2}, f_{j3}, ..., f_{jD}\}$ 'a best' represents global best particles index overall given particles. Each particle moves over a wave of optimum particles determined by 'pre-good' and 'a-best'. The initial wave of particles is selected randomly. Each particle uses the memory gained by it in the swarm to move towards the best solution. The population considered in PSO is binary. A '1' represents that the feature has been selected and a '0' represents that the feature has been discarded.

2.3.2 Genetic search (GS)

Genetic search is a search-based algorithm used for feature selection [38]. Genetic algorithm is widely used to obtain optimized solutions using mutation and crossover. In the crossover, a pair of offspring chromosome is produced by the combination of two-parent

chromosomes. Mutation is a process for maintaining genetic diversity from one generation to another. It alters one or more gene values in a chromosome from its initial state. It is a meta-heuristic approach that depends on the selection process of evolutionary algorithms. The performance of the Genetic algorithm (GA) depends on search space (SS), fitness function (FF), selection crossover, and mutation. SS is the set containing all possible solutions. Each value of SS shows one possible solution. A value or fitness is assigned to each solution of SS. Each feasible solution can be named as individual or chromosomes. FF is used to measure how close a chromosome is to the desired objective function.

2.3.3 Linear forward selection (LFS)

LFS is an iterative method that uses Hill climbing search initiate [11]. In the first iteration, this method evaluates each feature for inclusion in the subset. The attribute, which gives maximum performance is included in the subset permanently. The search is terminated when the inclusion of no single attribute helps in improving the current best performance. LFS starts with an empty subspace and calculates the attributes by using selected features. To select the highest value features are based on good attributes.

The general proposition that helps in understanding the concept of removal of redundant or irrelevant features can be understood from the following theorem [17].

2.3.4 Theorem: the spanning set theorem

Let $S = \{v_1, v_2, v_3, ...v_p\}$ be a set in a feature vector space V, and let $H = Span\{v_1, v_2, v_3, ...v_p\}$.

a. If one of the vectors in $S - say\ v_k$ is a linear combinition of vectors in S, then the set formed from S by removing v_k still spans H.

b. If $H \neq \{0\}$, some subset of H is a basis for H.

Proof a. By rearranging the list of vectors in S, if necessary, we may suppose that v_p is a linear combination of $v_1, ..., v_{p-1}$—say,

$$v_p = a_1 v_1 + \cdots + a_{p-1} v_{p-1}. \tag{1}$$

□

Given any x in H, we may write

$$x = c_1 v_1 + \cdots + c_{p-1} v_{p-1} + c_p v_p, \tag{2}$$

for suitable scalars $c_1, ..., c_p$.

Substituting the expression for v_p from (1) into (2), it is easy to see that x is a linear combination of $v_1, ..., v_{p-1}$.

Thus $\{v_1, ..., v_{p-1}\}$ spans H, because x was an arbitrary element of H.

b. If the original spanning set S is linearly independent, then it is already a basis for H.

Otherwise, one of the vectors in S depends on the others and can be deleted, by part (a). So long as there are two or more vectors in the spanning set, we can repeat this process until the spanning set is linearly independent and hence is a basis for H. If the spanning set is eventually reduced to one vector, that vector will be nonzero (and hence linearly independent) because $H \neq \{0\}$.

A example that shows application of the above theorem is geien as,

EXAMPLE: A basis is an "efficient" spanning set that contains no unnecessary vectors. In fact, a basis can be constructed from a spanning set by discarding unneeded vectors. For e.g.,

$$\text{Let } v_1 = \begin{bmatrix} 0 \\ 2 \\ .1 \end{bmatrix}, v_2 = \begin{bmatrix} 2 \\ 2 \\ 0 \end{bmatrix}, v_3 = \begin{bmatrix} 6 \\ 16 \\ .5 \end{bmatrix}$$

and $H = Span\{v_1, v_2, v_3\}$.

Note that $v_3 = 5v_1 + 3v_2$, and show that $Span\{v_1, v_2, v_3\} = Span\{v_1, v_2\}$. Then find a basis for the subspace H.

SOLUTION: Every vector in $Span\{v_1, v_2\}$ belongs to H because $c_1v_1 + c_2v_2 = c_1v_1 + c_2v_2 + 0v_3$.

Now let x be any vector in H—say, $x = c_1v_1 + c_2v_2 + c_3v_3$. Since $v_3 = 5v_1 + 3v_2$, we may substitute

$x = c_1v_1 + c_2v_2 + c_3(5v_1 + 3v_2) = (c_1 + 5c_3)v_1 + (c_2 + 3c_3)v_2$. Thus x is in $Span\{v_1, v_2\}$, so every vector in H already belongs to $Span\{v_1, v_2\}$. We conclude that H and $Span\{v_1, v_2\}$ are actually the same set of vectors. It follows that $\{v_1, v_2\}$ is a basis of H since $\{v_1, v_2\}$ is obviously linearly independent.

After feature selection is performed, the selected features are given as input to a SVR model for the prediction of image quality score. SVR is implemented using the LibSVM package.

3 Experimental results

3.1 Databases

The performance of the proposed methodology has been evaluated on two publicly available datasets i.e., MDID2017 [41] and LIVEMD [12]. LIVE multiply distorted image database (LIVEMD) consists of 15 reference images and a total of 450 distorted images that are divided into two groups of multiple distortions, the first group has blur followed by JPEG compression and the second group contains blur followed by JPEG noise. A maximum of 19 observers evaluated the images to compute their quality score. The multiple distorted image dataset (MDID2017) consists of 20 reference images and 1600 distorted images, five types of distortions are included i.e., Gaussian noise, Gaussian blur, contrast change, JPEG, and JPEG2000. A total of 192 subjects evaluated the images to compute the subjective quality score of images. The TID2013 database has a total of 3000 images with 25 pristine images and 24 distortion types [35]. The CSIQ database consists of 1162 images in total, with 5 distortion types and 30 pristine images [16]. The SIQAD database has a total of 980 images with 7 distortion types and 20 pristine images [47].

3.2 Performance parameters

Using NR-IQA techniques, features are computed for the images in the datasets. The images are divided into two sets i.e., training and testing. 80% images are randomly selected for training and 20% images are randomly selected for testing over 1000 iterations. The training and testing sets are selected such that no overlapping exists between the training and testing datasets, which means that the images present in the training set are not present in the testing set. WEKA tool is used to implement feature selection algorithms GS, PSO, and

LFS. Four performance parameters are used: Spearman's ranked ordered correlation constant (SROCC), linear correlation constant (LCC), Kendall correlation constant (KCC), and root-mean-squared error (RMSE). SROCC is computed as,

$$SROCC = 1 - \frac{6\Sigma x_t^2}{m(m^2-1)}, \tag{3}$$

where x_t is the difference between paired ranks and m is the total number of observations. LCC is computed as:

$$LCC = \frac{\sum_{j=1}^{m}(a_j - \bar{b})(c_j - \bar{c}))}{\sqrt{\sum_{j=1}^{m}(b_j - \bar{b})^2}\sqrt{\sum_{j=1}^{m}(c_j - \bar{c})^2}}, \tag{4}$$

where b_j and c_j are the values in first dataset and second dataset respectively, and $\bar{b}$ and $\bar{c}$ are mean values of b_j and c_j respectively. KCC is computed as follows,

$$KCC = \frac{m_x - m_y}{m(m-1)/2}, \tag{5}$$

where m is the total number of observations, m_x is the number of concordant pairs, and m_y is the number of discordant pairs. Fourth parameter, RMSE is computed as:

$$RMSE = \frac{1}{n}\sqrt{\sum_{i=1}^{n}(x_{dmos} - x_{score})^2}, \tag{6}$$

where x_{dmos} is MOS and x_{score} is the image quality score.

3.3 Performance comparison

Table 2 shows the performance comparison of features extracted using NR-IQA techniques and their combination on the LIVEMD database. It can be observed that when single NR-IQA technique is considered DIIVINE is ranked top, BRISQUE is ranked second, BLIINDS-II is ranked third, GM-LOG is ranked fourth, CurveletQA is ranked fifth and SSEQ is ranked sixth with SROCC scores 0.9319, 0.9233, 0.9097, 0.9053, 0.9047, 0.8938 respectively. When a combination of features fused using two NR-IQA techniques at a time are considered, the performance improves and C92 is ranked top with a SROCC score of 0.9470, C22 is ranked second with a SROCC score of 0.9458 and C42 is ranked third with a SROCC score of 0.9454. The performance improves further when a combination of features from three NR-IQA techniques are considered and C33 is ranked top, C123 is ranked second, and C153 is ranked third with SROCC scores of 0.9527, 0.9506 and 0.9462 respectively. When features from four NR-IQA techniques are considered at a time, the performance again improves and C134 is ranked top with a SROCC score of 0.9530, C154 is ranked second with a SROCC score of 0.9458 and C54 is ranked third with a SROCC score of 0.9451. The performance over LIVEMD database improves further when feature fusion is performed using five NR-IQA techniques at a time, with C45 ranked top with SROCC score of 0.9555, C35 ranked at second position with SROCC score of 0.9381, C65 is ranked at third position with a SROCC score of 0.9364. The performance remains the same with a SROCC score of 0.9555 when features are fused for all six NR-IQA techniques are considered.

Table 2 Performance comparison of the proposed methodology using all combinations of feature level fusion on LIVEMD database in terms of median values of SROCC, LCC, KCC and RMSE over 1000 runs

Feature combination	Combination symbol	SROCC	LCC	KCC	RMSE
BRISQUE	BRSQ	0.9233	0.9413	0.7717	6.5961
CURVELETQA	CQA	0.9047	0.9299	0.7448	7.1405
DIIVINE	DIV	**0.9319**	**0.9452**	**0.7812**	**6.3735**
GM-LOG	GLOG	0.9053	0.9198	0.7367	7.6492
SSEQ	SSEQ	0.8938	0.9189	0.7293	7.6512
BLIINDS-II	BLND2	0.9097	0.9308	0.7489	7.0800
BRSQ,CQA	C12	0.9370	0.9527	0.7954	5.9412
BRSQ,DIV	C22	0.9458	0.9590	0.8121	5.4803
BRSQ,SSEQ	C42	0.9454	0.9583	0.8115	5.5895
BLND2,BRSQ	C52	0.9388	0.9536	0.7954	5.8876
CQA,DIV	C62	0.9424	0.9540	0.8040	5.8542
BLND2,CQA	C92	**0.9470**	**0.9602**	**0.8135**	**5.4471**
BRSQ,GLOG	C32	0.9250	0.9262	0.7751	6.2131
BLND2,DIV	C122	0.9342	0.9473	0.7831	6.2711
BLND2,GLOG	C132	0.9110	0.9321	0.7495	7.0100
BLND2,SSEQ	C152	0.9108	0.9318	0.7510	7.0510
CQA,GLOG	C72	0.9060	0.9312	0.7461	7.0121
CQA,SSEQ	C82	0.9061	0.9305	0.7462	7.1010
DIV,GLOG	C102	0.9321	0.9460	0.7824	6.3150
DIV,SSEQ	C112	0.9330	0.9471	0.7842	6.3410
GLOG,SSEQ	C142	0.9061	0.9206	0.7375	7.6482
BRSQ,CQA,DIV	C13	0.9455	0.9592	0.8101	5.4668
BLND2,BRSQ,CQA	C33	**0.9527**	**0.9651**	**0.8236**	**5.1346**
BRSQ,CQA,SSEQ	C43	0.9446	0.9584	0.8081	5.5777
CQA,DIV,SSEQ	C73	0.9428	0.9578	0.8055	5.5968
BLND2,CQA,SSEQ	C123	0.9506	0.9629	0.8216	5.2629
BLND2,CQA,GLOG	C133	0.9435	0.9583	0.8061	5.5933
CQA,GLOG,SSEQ	C143	0.9384	0.9560	0.7997	5.7435
BLND2,BRSQ,SSEQ	C153	0.9462	0.9601	0.8115	5.4415
BRSQ,GLOG,SSEQ	C173	0.9428	0.9578	0.8055	5.5968
BLND2,BRSQ,DIV	C183	0.9391	0.9561	0.8000	5.7259
BRSQ,DIV,SSEQ	C193	0.9408	0.9569	0.8040	5.6129
DIV,GLOG,SSEQ	C93	0.9345	0.9465	0.7836	6.2910
CQA,DIV,GLOG	C53	0.9333	0.9465	0.7845	6.2109
BLND2,GLOG,SSEQ	C103	0.9105	0.9315	0.7501	7.0200
BLND2,DIV,SSEQ	C113	0.9338	0.9470	0.7861	6.2911
BLND2,DIV,GLOG	C83	0.9360	0.9471	0.7831	6.3115
BLND2,CQA,DIV	C63	0.9327	0.9458	0.7818	6.3512
BRSQ,DIV,GLOG	C203	0.9337	0.9468	0.7828	6.3121
BRSQ,CQA,GLOG	C23	0.9245	0.9431	0.7729	6.3123
BLND2,BRSQ,GLOG	C163	0.9240	0.9420	0.7724	6.5161
BLND2,BRSQ,CQA,DIV	C24	0.9433	0.9574	0.8062	5.6442

Table 2 (continued)

Feature combination	Combination symbol	SROCC	LCC	KCC	RMSE
BRSQ,CQA,DIV,SSEQ	C34	0.9426	0.9567	0.8061	5.6603
BLND2,CQA,GLOG,SSEQ	C54	0.9451	0.9604	0.8101	5.4057
BLND2,BRSQ,GLOG,SSEQ	C94	0.9415	0.9565	0.8020	5.7029
BLND2,BRSQ,CQA,SSEQ	C134	**0.9530**	**0.9629**	**0.8236**	**5.2627**
BLND2,BRSQ,CQA,GLOG	C144	0.9444	0.9600	0.8095	5.4603
BRSQ,CQA,GLOG,SSEQ	C154	0.9458	0.9609	0.8135	5.3793
CQA,DIV,GLOG,SSEQ	C84	0.9335	0.9471	0.7841	6.2914
BLND2,DIV,GLOG,SSEQ	C44	0.9359	0.9492	0.7852	6.1910
BLND2,CQA,DIV,SSEQ	C64	0.9365	0.9451	0.7861	6.2735
BLND2,CQA,DIV,GLOG	C74	0.9371	0.9491	0.7861	6.1211
BRSQ,DIV,GLOG,SSEQ	C124	0.9391	0.9501	0.7871	6.0502
BRSQ,CQA,DIV,GLOG	C14	0.9397	0.9499	0.7889	6.0211
BLND2,BRSQ,DIV,SSEQ	C104	0.9376	0.9975	0.7835	6.2912
BLND2,BRSQ,DIV,GLOG	C114	0.9361	0.9492	0.7862	6.0101
BLND2,BRSQ,CQA,DIV,SSEQ	C35	0.9381	0.9538	0.7980	5.8495
BLND2,BRSQ,CQA,GLOG,SSEQ	C45	**0.9555**	**0.9703**	**0.8262**	**5.0180**
BLND2,CQA,DIV,GLOG,SSEQ	C65	0.9364	0.9538	0.7939	5.8513
BLND2,BRSQ,CQA,DIV,GLOG	C15	0.9321	0.9454	0.7814	6.3635
BLND2,BRSQ,DIV,GLOG,SSEQ	C55	0.9325	0.9458	0.7816	6.3312
BRSQ,CQA,DIV,GLOG,SSEQ	C25	0.9329	0.9462	0.7822	6.2113
BRQ,BLND2,CQA,DIV,GLOG,SSEQ	C16	**0.9555**	**0.9703**	**0.8262**	**5.0180**

Table 3 shows the performance of NR-IQA techniques and their combinations on the MDID2017 database. DIIVINE is raked top with a SROCC score of 0.9019, BRISQUE is ranked second with a SROCC score of 0.8676, and BLIINDS-II is ranked third with a SROCC score of 0.8496 when features from a single NR-IQA technique is considered at the time. It can be observed that the performance improves when a combination of features from two NR-IQA techniques at a time is considered. C92 shows the best performance, C22 is ranked second and C42 is ranked third with SROCC scores of 0.9416, 0.9380, and 0.9344 respectively. The combination of features from three NR-IQA techniques further improve the performance with C33 ranked a top position, C13 ranked second and C153 ranked third with a SROCC score of 0.9497, 0.9445, and 0.9435 respectively. The performance further improves when features are fused using four NR-IQA techniques. C134 performs the best with a SROCC score of 0.9519, C154 is ranked second with a SROCC score of 0.9481, and C54 is ranked third with a SROCC score of 0.9458. When feature fusion is performed using five NR-IQA techniques at a time, the best performance is achieved with C55 that has a SROCC score of 0.9587, C35 is ranked second with a SROCC score of 0.9532, and C65 is ranked third with a SROCC score of 0.9494. The performance does not improve further when feature fusion is performed using all six NR-IQA techniques and the SROCC score remains at 0.9587.

Table 4 shows the performance of the combination of features using six different NR-IQA techniques with three feature selection algorithms i.e., GS, PSO, and LFS over the

Table 3 Performance comparison of the proposed methodology using all combinations of feature level fusion on MDID2017 database in terms of median values of SROCC, LCC, KCC and RMSE over 1000 runs

Feature combination	Combination symbol	SROCC	LCC	KCC	RMSE
BRISQUE	BRSQ	0.8676	0.8672	0.6746	1.1009
CURVELETQA	CQA	0.8109	0.8124	0.6155	1.2899
DIIVINE	DIV	**0.9019**	**0.9038**	**0.7300**	**0.9471**
GM-LOG	GLOG	0.8315	0.8315	0.6334	1.2284
SSEQ	0.7620	0.7664	0.5635	2.3837	
BLIINDS-II	BLND2	0.8496	0.8497	0.6566	1.1662
BRSQ,DIV	C22	0.9380	0.9370	0.7856	0.7769
CQA,SSEQ	C82	0.9114	0.9061	0.7341	0.8154
DIV,SSEQ	C112	0.8843	0.8860	0.6975	1.0238
BLND2,DIV	C122	0.8741	0.8792	0.6805	1.1294
BLND2,BRSQ	C52	0.9250	0.9250	0.7651	0.8387
BRSQ,CQA	C12	0.9202	0.9175	0.7830	1.5434
BRSQ,GLOG	C32	0.8868	0.8827	0.6857	1.0120
BRSQ,SSEQ	C42	0.9344	0.9341	0.7786	0.7933
BLND2,CQA	C92	**0.9416**	**0.9419**	**0.7938**	**0.7463**
BLND2,GLOG	C132	0.8440	0.8465	0.6454	1.1758
BLND2,SSEQ	C152	0.8789	0.8784	0.6901	1.0576
CQA,DIV	C62	0.9275	0.9285	0.7671	0.8215
CQA,GLOG	C72	0.8280	0.8286	0.6260	1.2986
DIV,GLOG	C102	0.9119	0.9191	0.7430	0.9315
GLOG,SSEQ	C142	0.9031	0.9058	0.73171	0.9351
BRSQ,CQA,DIV	C13	0.9445	0.9439	0.7972	0.7339
BLND2,CQA,DIV	C63	0.9382	0.9384	0.7875	0.7606
CQA,DIV,SSEQ	C73	0.9075	0.9082	0.7314	0.9256
BLND2,DIV,SSEQ	C113	0.9360	0.9306	0.7913	0.5357
BLND2,CQA,SSEQ	C123	0.9429	0.9427	0.7927	0.7392
BLND2,CQA,GLOG	C133	0.9425	0.9415	0.7919	0.7497
DIV,GLOG,SSEQ	C93	0.9027	0.9051	0.7346	0.8884
CQA,GLOG,SSEQ	C143	0.9250	0.9271	0.7682	0.8290
CQA,DIV,GLOG	C53	0.8912	0.8979	0.6986	0.9356
BLND2,GLOG,SSEQ	C103	0.9012	0.9079	0.7340	0.9010
BLND2,DIV,GLOG	C83	0.9033	0.9065	0.7390	0.8874
BRSQ,GLOG,SSEQ	C173	0.9297	0.9311	0.7718	0.8077
BRSQ,DIV,SSEQ	C193	0.9028	0.9067	0.7351	0.8886
BRSQ,DIV,GLOG	C203	0.9022	0.9077	0.7389	0.8960
BRSQ,CQA,SSEQ	C43	0.9391	0.9408	0.7891	0.7491
BRSQ,CQA,GLOG	C23	0.8712	0.8735	0.6793	1.0744
BLND2,BRSQ,SSEQ	C153	0.9435	0.9452	0.7081	0.5686
BLND2,BRSQ,GLOG	C163	0.8942	0.8952	0.7103	0.9833
BLND2,BRSQ,DIV	C183	0.9145	0.9150	0.7395	0.8089
BLND2,BRSQ,CQA	C33	**0.9497**	**0.9500**	**0.8089**	**0.6934**
BLND2,BRSQ,CQA,DIV	C24	0.9444	0.9404	0.8095	0.5857

Table 3 (continued)

Feature combination	Combination symbol	SROCC	LCC	KCC	RMSE
BLND2,CQA,GLOG,SSEQ	C54	0.9458	0.9559	0.8135	0.7193
CQA,DIV,GLOG,SSEQ	C84	0.9109	0.9156	0.7346	0.8203
BLND2,BRSQ,GLOG,SSEQ	C94	0.9415	0.9467	0.8020	0.6603
BLND2,BRSQ,CQA,SSEQ	C134	**0.9519**	**0.9522**	**0.8100**	**0.6761**
BLND2,BRSQ,CQA,GLOG	C144	0.9451	0.9450	0.8101	0.6603
BRSQ,CQA,GLOG,SSEQ	C154	0.9481	0.9485	0.8052	0.7022
BLND2,DIV,GLOG,SSEQ	C44	0.9102	0.9156	0.7342	0.8155
BLND2,CQA,DIV,SSEQ	C64	0.9182	0.9196	0.7399	0.8059
BLND2,CQA,DIV,GLOG	C74	0.9136	0.9155	0.7374	0.8087
BRSQ,DIV,GLOG,SSEQ	C124	0.9118	0.9166	0.7350	0.8196
BRSQ,CQA,DIV,SSEQ	C34	0.9433	0.9474	0.8061	0.6442
BRSQ,CQA,DIV,GLOG	C14	0.9112	0.9164	0.7383	0.8190
BLND2,BRSQ,DIV,SSEQ	C104	0.9100	0.9141	0.7338	0.8160
BLND2,BRSQ,DIV,GLOG	C114	0.9145	0.9149	0.7346	0.8091
BLND2,BRQ,CQA,DIV,GLOG	C15	0.9300	0.9340	0.7339	0.8000
BLND2,BRSQ,CQA,DIV,SSEQ	C35	0.9532	0.9529	0.8133	0.6732
BLND2,BRSQ,CQA,GLOG,SSEQ	C45	**0.9587**	**0.9588**	**0.8246**	**0.6296**
BLND2,CQA,DIV,GLOG,SSEQ	C65	0.9494	0.9487	0.8033	0.7027
BLND2,BRSQ,DIV,GLOG,SSEQ	C55	0.9309	0.9356	0.7346	0.7992
BRSQ,CQA,DIV,GLOG,SSEQ	C25	0.9455	0.9503	0.8112	0.5480
BRSQ,BLND2,CQA,DIV,GLOG,SSEQ	C16	**0.9587**	**0.9588**	**0.8246**	**0.6296**

LIVEMD database. Results are reported for feature selection applied over the top six performing feature fusion combinations in each category. When feature selection is applied over single NR-IQA techniques DIV-GS performs the best whereas, DIIVINE without feature selection is ranked second and BRSQ-GS is ranked third with SROCC scores 0.9393, 0.9319, and 0.9306 respectively. When feature fusion is performed using features from two NR-IQA techniques at a time with feature selection the performance is improved and C92-GS is ranked top with a SROCC score of 0.9557, C22-GS is ranked second with a SROCC score of 0.9503, and C42-GS is ranked third with a SROCC score of 0.9485. It is observed that the performance further improves when a combination of feature fusion from three NR-IQA techniques are considered at a time. C33-GS is ranked top with a SROCC score of 0.9619, C123-GS is ranked second with a SROCC score of 0.9556, and C33 is ranked third with a SROCC score of 0.9527. The performance further improves when features are fused from four NR-IQA techniques and feature selection is performed. C134-GS is ranked top, C154-GS is ranked second and C134-PSO is ranked third with SROCC scores of 0.967, 0.9541, and 0.9524 respectively. Improvement in performance is measured by the higher correlation between predicted and subjective quality scores when feature fusion is performed using features from five different NR-IQA techniques at one time. C45-GS is ranked top with a SROCC score of 0.9691, C35-GS is ranked second with a SROCC score of 0.9537 and C25-GS is ranked third with a SROCC score of 0.9516. The performance does not improve further if we fuse all the features of six NR-IQA techniques. In terms of execution time, it can be observed that the least execution time is consumed by SSEQ-GS,

Table 4 Performance comparison of the proposed methodology using feature level fusion and feature selection on the LIVEMD database in terms of median values of SROCC, LCC, KCC, RMSE, MAE (mean absolute error) and execution time over 1000 runs

Combination symbol	SROCC	LCC	KCC	RMSE	MAE	Execution time
BRSQ-GS	0.9306	0.9413	0.7812	6.5961	5.0209	35.2400
BRSQ-PSO	0.8853	0.913	0.7125	7.9619	6.2662	30.0961
BRSQ-LFS	0.8814	0.9108	0.7027	8.0296	6.4101	25.9918
BLND2-GS	0.9120	0.9291	0.7448	7.1405	5.3917	31.6875
BLND2-PSO	0.8911	0.9189	0.7232	7.6512	5.9509	30.8281
BLND2-LFS	0.8826	0.912	0.7105	7.9723	6.3235	24.7182
CQA-GS	0.9173	0.9308	0.7489	7.0324	5.2361	26.3651
CQA-PSO	0.8373	0.8787	0.6505	9.2772	7.3009	23.6945
CQA-LFS	0.8725	0.9067	0.6943	8.1112	6.4707	25.4530
DIV-GS	**0.9393**	**0.9506**	**0.7932**	**6.3867**	**4.8158**	**64.6110**
DIV-PSO	0.9124	0.9299	0.7475	7.08	5.3121	56.8449
DIV-LFS	0.8656	0.8933	0.6848	8.7749	6.8522	35.7573
GLOG-GS	0.9195	0.9363	0.7543	6.9431	5.1202	30.9574
GLOG-PSO	0.8906	0.9183	0.7232	7.6899	5.9562	31.0858
GLOG-LFS	0.8666	0.8993	0.6909	8.4961	6.8113	25.9694
SSEQ-GS	0.9066	0.9267	0.7367	7.4161	5.8568	21.2308
SSEQ-PSO	0.8666	0.8993	0.6909	8.4961	6.8113	21.2308
SSEQ-LFS	0.8666	0.8993	0.6909	8.4961	6.8113	21.2308
C22-GS	0.9503	0.9602	0.8182	5.2091	4.1624	78.7168
C22-PSO	0.9461	0.9583	0.8110	5.5895	4.3247	68.3055
C22-LFS	0.9111	0.9311	0.7535	6.9800	5.4451	41.0700
C42-GS	0.9485	0.9592	0.8135	5.4471	4.1999	69.6705
C42-PSO	0.9386	0.9515	0.7954	5.9412	4.6639	64.4183
C42-LFS	0.9238	0.9344	0.7664	6.8342	5.3367	42.9722
C92-GS	**0.9557**	**0.9853**	**0.8285**	**5.0607**	**4.011**	**35.5981**
C92-PSO	0.9063	0.928	0.7489	7.2546	5.6178	35.3894
C92-LFS	0.9106	0.9309	0.7489	7.0622	5.4851	30.9332
C12-GS	0.9446	0.9540	0.8034	5.7899	4.4789	79.0657
C12-PSO	0.9372	0.9458	0.7939	5.9521	4.7077	77.1954
C12-LFS	0.8988	0.9184	0.7313	7.6924	5.9481	43.9767
C52-GS	0.9466	0.9583	0.8115	5.5818	4.3095	65.8377
C52-PSO	0.9257	0.9358	0.7711	6.817	5.2437	59.4493
C52-LFS	0.8839	0.9113	0.7091	8.0243	6.3395	37.2664
C62-GS	0.9438	0.9536	0.8019	5.8542	4.4834	75.0096
C62-PSO	0.9366	0.9534	0.7954	5.8694	4.5817	72.7077
C62-LFS	0.8995	0.9257	0.7347	7.3069	5.7018	41.8869
C123-GS	0.9556	0.9651	0.8297	5.1346	3.9581	85.7911
C123-PSO	0.9525	0.9629	0.8236	5.2429	4.0382	76.0399
C123-LFS	0.9384	0.9518	0.7974	5.9404	4.5623	48.7003
C33-GS	**0.9619**	**0.9675**	**0.8298**	**5.0012**	**3.8432**	**50.6887**
C33-PSO	0.9154	0.9357	0.7610	6.8447	5.2922	44.6919

Table 4 (continued)

Combination symbol	SROCC	LCC	KCC	RMSE	MAE	Execution time
C33-LFS	0.9263	0.9450	0.7758	6.3695	4.9524	36.1115
C153-GS	0.9503	0.9617	0.8214	5.3074	4.1469	85.6336
C153-PSO	0.9473	0.9592	0.8135	5.4845	4.2921	82.4552
C153-LFS	0.9358	0.9512	0.7939	5.9578	4.5623	52.5707
C13-GS	0.9502	0.9614	0.8190	5.3485	4.1764	82.3259
C13-PSO	0.9439	0.9565	0.8061	5.6975	4.5159	77.9750
C13-LFS	0.9250	0.9398	0.7731	6.6025	5.1410	47.7123
C43-GS	0.9498	0.9601	0.8167	5.4415	4.2546	73.6941
C43-PSO	0.9384	0.9518	0.7974	5.9404	4.5623	66.4029
C43-LFS	0.9251	0.9398	0.7731	6.6025	5.1410	44.6013
C133-GS	0.9487	0.9604	0.8176	5.4035	4.238	90.6618
C133-PSO	0.9448	0.9583	0.8081	5.5933	4.4561	81.5635
C133-LFS	0.9193	0.9367	0.7650	6.8010	5.2722	44.8384
C54-GS	0.9511	0.9625	0.8222	5.2642	4.1248	100.004
C54-PSO	0.9487	0.9604	0.8176	5.4035	4.2380	90.177
C54-LFS	0.9441	0.9597	0.8095	5.4603	4.4460	58.846
C154-GS	0.9541	0.9632	0.8263	5.2145	4.0054	101.132
C154-PSO	0.9498	0.961	0.8182	5.3793	4.1849	86.9494
C154-LFS	0.9406	0.9539	0.8014	5.8396	4.5785	54.8230
C134-GS	**0.9670**	**0.9641**	**0.8303**	**5.1924**	**3.9646**	**86.5435**
C134-PSO	0.9524	0.963	0.8242	5.2287	4.0468	77.5237
C134-LFS	0.9366	0.9534	0.7954	5.8694	4.5817	49.0454
C24-GS	0.9506	0.9615	0.8216	5.3355	4.1543	86.3273
C24-PSO	0.9441	0.9597	0.8095	5.4603	4.4460	80.6158
C24-LFS	0.9252	0.9406	0.7737	6.5591	5.0945	50.1331
C34-GS	0.9498	0.961	0.8182	5.3793	4.1849	96.9081
C34-PSO	0.9502	0.9614	0.8190	5.3485	4.1764	92.2841
C34-LFS	0.9327	0.9503	0.7879	6.0503	4.6725	58.4650
C144-GS	0.9509	0.9623	0.822	5.2868	4.1477	85.8912
C144-PSO	0.9476	0.9603	0.8141	5.4057	4.2651	83.1330
C144-LFS	0.9356	0.951	0.7939	5.9573	4.6325	53.5228
C144-GS	0.9507	0.9626	0.8202	5.2593	4.1321	116.245
C144-PSO	0.9500	0.9621	0.8190	5.3101	4.1892	102.712
C144-LFS	0.9407	0.9579	0.8049	5.5717	4.3638	63.5240
C25-GS	0.9516	0.9629	0.8212	5.2452	4.1190	100.681
C25-PSO	0.9487	0.9604	0.8176	5.418	4.2052	90.927
C25-LFS	0.9435	0.9596	0.8101	5.4512	4.3589	58.314
C35-GS	0.9537	0.9633	0.8222	5.2434	4.1042	99.0460
C35-PSO	0.9496	0.9609	0.8182	5.4008	4.2015	86.4783
C35-LFS	0.9399	0.9545	0.8014	5.7896	4.4642	54.2752
C45-GS	**0.9691**	**0.9768**	**0.8293**	**4.9400**	**3.9107**	**63.6820**
C45-PSO	0.9278	0.9454	0.7778	6.3635	4.914	59.9632
C45-LFS	0.9298	0.9458	0.7816	6.3258	4.7342	44.0903

Table 4 (continued)

Combination symbol	SROCC	LCC	KCC	RMSE	MAE	Execution time
C55-GS	0.9479	0.9602	0.8141	5.4474	4.2587	103.021
C55-PSO	0.9482	0.9603	0.8141	5.4389	4.2371	96.348
C55-LFS	0.9280	0.9456	0.7814	6.3312	4.7880	55.284
C65-GS	0.9497	0.9613	0.8182	5.3516	4.1917	96.6957
C65-PSO	0.9504	0.9622	0.8200	5.3089	4.1483	92.9299
C65-LFS	0.9327	0.9497	0.7859	6.0857	4.6684	57.2327
C16-GS	**0.9691**	**0.9768**	**0.8293**	**4.9400**	**3.9107**	**109.0234**
C16-PSO	0.9278	0.9454	0.7778	6.3635	4.914	101.83792
C16-LFS	0.9298	0.9458	0.7816	6.3258	4.7342	62.2155

SSEQ-PSO, and SSEQ-LFS i.e., 21.2308 seconds. The largest execution time is used by C16 i.e., 203.6119 seconds. The execution time of best performing C45-GS and C16-GS is 63.6820 and 109.0234 seconds respectively.

Table 5 shows the performance of features extracted using six differnt NR-IQA techniques and their combinations with three feature selection algorithms i.e., GS, PSO, and LFS over the MDID2017 database. It can be observed that DIV-GS performs the best with a SROCC score of 0.9093, DIV-PSO is ranked second with a SROCC score of 0.8824, and BRSQ-GS is ranked third with a SROCC score of 0.8749. The performance improves when combinations of features fused using two NR-IQA techniques at a time are considered. C92-GS performs best, C42-GS is ranked second and C22-GS is ranked third with SROCC scores of 0.9503, 0.9475, and 0.9425 respectively. It can be observed that the performance improves further, when feature fusion is performed using features from three NR-IQA techniques at a time with C33-GS ranked at the top position achieving a SROCC score of 0.9589, C33 performs second best with a SROCC score of 0.9497, and C13-GS is ranked third with a SROCC score of 0.9492. The feature fusion performed using features from four NR-IQA techniques considered at a time help in improving the performance further, and C134-GS is ranked at the top position, C154-GS is ranked second and C134-PSO is ranked third with SROCC scores 0.9669, 0.9564 and 0.9523 respectively. Using feature fusion from features of five NR-IQA techniques at a time, further improve the performance with C35-GS ranked at the top with a SROCC score of 0.9723, C35-GS is ranked second with a SROCC score of 0.9688, and C35-PSO is ranked third with a SROCC score of 0.9647. The performance does not improve further when features are fused from all six NR-IQA techniques. In terms of execution time, the largest execution time of 45.4905 is consumed by C16, while the lowest execution time of 4.52920 seconds is consumed by SSEQ-GS, SSEQ-PSO, and SSEQ-LFS. The combination with the highest performance i.e., C45-GS and C16-GS have an execution time of 13.5854 and 25.0990 seconds respectively.

Table 6 shows the overall performance of the features extracted using six differnt NR-IQA techniques and their combinations with three feature selection algorithms i.e., GS, PSO, and LFS over the MDID2017 and LIVEMD databases. It can be observed that DIV-GS shows the best performance with a SROCC score of 0.9162, DIIVINE is ranked second and DIV-PSO is ranked third when single NR-IQA technique and feature selection is considered. The performance improves when features are fused considering combination features from two NR-IQA techniques. C92-GS is ranked top with a SROCC score of 0.9515, whereas C42-GS is ranked second and C92 is ranked third with a SROCC score of 0.9477 and 0.9428

Table 5 Performance comparison of the proposed methodology for feature level fusion and feature selection on the MDID2017 database in terms of median values of SROCC, LCC, KCC, RMSE, MAE (mean absolute error) and execution time over 1000 runs

Combination symbol	SROCC	LCC	KCC	RMSE	MAE	Execution time
BRSQ-GS	0.8749	0.8765	0.6961	1.0525	3.7876	7.51780
BRSQ-PSO	0.8296	0.8395	0.6202	1.4168	4.3976	6.42040
BRSQ-LFS	0.8257	0.8367	0.6196	1.7295	4.4631	5.54490
BLND2-GS	0.8519	0.8519	0.651	1.1059	3.927	6.75990
BLND2-PSO	0.8310	0.8416	0.6309	1.2634	4.3959	6.57660
BLND2-LFS	0.8225	0.8319	0.6134	1.8006	4.46715	5.27320
CQA-GS	0.8235	0.833	0.6187	1.7761	4.46715	5.62450
CQA-PSO	0.7435	0.7595	0.5212	2.6455	5.24910	5.05480
CQA-LFS	0.7787	0.7818	0.5684	2.2067	4.807575	5.42990
DIV-GS	**0.9093**	**0.9092**	**0.7420**	**0.5223**	**3.61185**	**13.7836**
DIV-PSO	0.8824	0.8788	0.6963	0.9603	3.7656	12.1268
DIV-LFS	0.8356	0.8476	0.634	1.1837	4.3491	7.62820
GLOG-GS	0.8457	0.848	0.6415	1.1818	4.0437	6.60420
GLOG-PSO	0.8168	0.8184	0.6104	1.8148	4.5370	6.63160
GLOG-LFS	0.7928	0.7933	0.5838	2.1976	4.7426	5.54010
SSEQ-GS	0.7748	0.7742	0.5635	2.3837	4.8530	4.52920
SSEQ-PSO	0.7348	0.7442	0.5184	3.3485	5.2491	4.52920
SSEQ-LFS	0.7348	0.7442	0.5184	3.3485	5.2491	4.52920
C22-GS	0.9425	0.9419	0.7923	0.3965	3.1499	16.7928
C22-PSO	0.9383	0.9366	0.7859	0.5822	3.2435	14.5718
C22-LFS	0.9033	0.9079	0.7292	2.1838	4.113825	8.76150
C42-GS	0.9475	0.9445	0.7938	0.3599	3.1218	14.8630
C42-PSO	0.9276	0.9285	0.7690	0.8215	3.448425	13.7425
C42-LFS	0.9128	0.9131	0.7413	1.7681	3.932775	9.16730
C92-GS	**0.9503**	**0.9640**	**0.8088**	**0.2937**	**3.00825**	**7.59420**
C92-PSO	0.9009	0.9069	0.7276	2.3614	4.21335	7.54970
C92-LFS	0.9052	0.9089	0.7292	2.1334	4.083825	6.59900
C12-GS	0.9278	0.9294	0.7807	0.7869	3.3625	16.8673
C12-PSO	0.9204	0.9198	0.7610	1.2815	3.58755	16.4683
C12-LFS	0.8820	0.8929	0.6944	2.6597	4.461075	9.38160
C52-GS	0.9328	0.9297	0.7844	0.7611	3.3084	14.0453
C52-PSO	0.9119	0.9126	0.7408	1.9479	4.002525	12.6824
C52-LFS	0.8701	0.8827	0.6788	2.9754	4.754625	7.95010
C62-GS	0.9289	0.9295	0.7842	0.7769	3.3591	16.0020
C62-PSO	0.9217	0.9216	0.7651	0.9937	3.530775	15.5109
C62-LFS	0.8846	0.9024	0.7252	2.5538	4.27635	8.93580
C123-GS	0.9479	0.9457	0.8008	0.5686	3.0286	18.3020
C123-PSO	0.9450	0.9439	0.7972	0.6874	3.1782	16.2218
C123-LFS	0.9307	0.9301	0.7508	1.4167	3.599325	10.3893
C33-GS	**0.9589**	**0.9524**	**0.8151**	**0.4345**	2.8824	**10.8135**
C33-PSO	0.9124	0.9191	0.6905	2.4035	3.96915	9.53420

Table 5 (continued)

Combination symbol	SROCC	LCC	KCC	RMSE	MAE	Execution time
C33-LFS	0.9233	0.9245	0.718	1.9283	3.85575	7.70370
C153-GS	0.9479	0.9469	0.7182	0.4345	3.1101	18.2684
C153-PSO	0.9446	0.9439	0.7968	0.7339	3.19095	17.5904
C153-LFS	0.9331	0.9363	0.7602	1.1300	3.421725	11.2150
C13-GS	0.9492	0.9468	0.8073	0.5600	2.9943	17.5628
C13-PSO	0.9429	0.941	0.7945	1.0342	3.433875	16.6346
C13-LFS	0.9240	0.9299	0.7463	1.8696	3.7143	10.1786
C43-GS	0.9443	0.9421	0.7927	0.7491	3.2190	15.7213
C43-PSO	0.9329	0.9316	0.7515	1.4111	3.4827	14.1659
C43-LFS	0.9196	0.921	0.7101	1.9444	3.9129	9.51492
C133-GS	0.9477	0.9452	0.8005	0.6109	3.0737	19.3411
C133-PSO	0.9438	0.9416	0.7919	0.7497	3.3024	17.4001
C133-LFS	0.9183	0.9206	0.7081	1.9724	3.95415	9.56550
C54-GS	0.9518	0.9521	0.8182	0.5857	3.1107	21.3341
C54-PSO	0.9494	0.9515	0.8112	0.5958	3.19402	19.2377
C54-LFS	0.9448	0.9427	0.8095	0.7464	3.3990	12.5539
C154-GS	0.9564	0.957	0.8249	0.3761	3.0040	21.5748
C154-PSO	0.9521	0.9554	0.8210	0.4642	3.0456	18.5491
C154-LFS	0.9429	0.9423	0.7931	1.1050	3.3345	11.6955
C134-GS	0.9669	0.9578	0.8254	0.3324	2.97345	18.4625
C134-PSO	0.9523	0.9559	0.8228	0.3874	3.0351	16.5383
C134-LFS	0.9365	0.9404	0.7931	1.1050	3.43627	10.4630
C24-GS	0.9517	0.9517	0.8180	0.5888	3.1157	18.4164
C24-PSO	0.9452	0.9452	0.8100	0.7193	3.3238	17.1980
C24-LFS	0.9263	0.9236	0.7770	1.5006	3.82087	10.6950
C34-GS	0.9505	0.9508	0.8147	0.6491	3.1404	20.6736
C34-PSO	0.9509	0.951	0.8149	0.6442	3.13867	19.6872
C34-LFS	0.9334	0.936	0.7818	1.3531	3.50437	12.4725
C144-GS	0.9516	0.9511	0.8167	0.6004	3.1323	18.3234
C144-PSO	0.9483	0.9479	0.8114	0.6761	3.19882	17.7350
C144-LFS	0.9363	0.9369	0.7879	1.1573	3.47437	11.4181
C15-GS	0.9486	0.9503	0.8033	0.6466	3.2691	24.7990
C15-PSO	0.9479	0.9502	0.7973	0.6554	3.2728	21.9120
C15-LFS	0.9386	0.9447	0.7671	0.7960	3.5013	13.5517
C25-GS	0.9642	0.9624	0.8375	0.2181	3.0990	21.4786
C25-PSO	0.9613	0.9571	0.8276	0.3819	3.1437	19.3979
C25-LFS	0.9561	0.9558	0.8247	0.4883	3.1511	12.4404
C35-GS	0.9688	0.9654	0.8472	0.1653	3.07815	21.1297
C35-PSO	0.9647	0.9637	0.8391	0.2154	3.0892	18.4486
C35-LFS	0.9550	0.9536	0.8167	0.5480	3.1539	11.5786
C45-GS	**0.9723**	**0.9667**	**0.8502**	**0.1621**	**3.00802**	**13.5854**
C45-PSO	0.9310	0.9377	0.7574	0.923	3.5163	12.7921
C45-LFS	0.9330	0.9382	0.7671	0.9082	3.5047	9.40590

Table 5 (continued)

Combination symbol	SROCC	LCC	KCC	RMSE	MAE	Execution time
C55-GS	0.9463	0.9488	0.7762	0.7027	3.4344	21.9778
C55-PSO	0.9466	0.9499	0.7843	0.6732	3.3481	20.5543
C55-LFS	0.9264	0.934	0.7339	1.9374	3.6855	11.7939
C65-GS	0.9627	0.9591	0.8294	0.2608	3.1419	20.6283
C65-PSO	0.9634	0.9593	0.8329	0.2540	3.1112	19.8250
C65-LFS	0.9457	0.9487	0.7727	0.7516	3.4700	12.2096
C16-GS	**0.9723**	**0.9667**	**0.8502**	**0.1621**	**3.00802**	**25.0990**
C16-PSO	0.9310	0.9377	0.7574	0.923	3.5163	22.1121
C16-LFS	0.9330	0.9382	0.7671	0.9082	3.5047	13.9527

respectively. The performance further improves, when feature fusion is performed using features from three NR-IQA techniques at a time and C33-GS gives the best performance with a SROCC score of 0.9595. C33 is ranked second with a SROCC score of 0.9503 and, C123-GS and C153-GS are ranked third with a SROCC score of 0.9484. C134-GS gives the best performance when feature fusion is performed using the pool of features from four different NR-IQA techniques considered with a SROCC score of 0.9669. C154-GS is ranked second and C134-PSO is ranked third with a SROCC score of 0.9558 and 0.9523 respectively. The best performance is achieved when features fusion is performed using features from five NR-IQA techniques and C45-GS is ranked top with a SROCC score of 0.9715. C35-GS is ranked second with a SROCC score of 0.9653 and, C25-GS and C35-PSO are ranked third with a SROCC score of 0.9612. The performance remains the same when features are fused for all six NR-IQA techniques, and C16-GS performs best with a SROCC score of 0.9715.

It can be observed from Table 2 to Table 6 that fusing features extracted in different domains help in improving the overall performance for NR-IQA. The features extracted using BRISQUE in the spatial domain, BLIINDS-II in the DCT domain, curveletQA in the curvelet domain, GM-LOG that extracts features using edge information in the image and SSEQ extracts features in the spectral and spatial domain, when fused together show the best performance. Adding the features from DIIVINE does not improve the performance, which is expected because curvelet transform is derived from the wavelet transform and hence supposed to encompass the statistical characteristics of features extracted in wavelet transform. Hence features extracted in spatial, DCT, spectral and curvelet domain, when fused together show the best performance.

Figure 2 summarizes the overall performance of the proposed methodology in terms of the SROCC score. The x-axis shows the feature vector used and the y-axis shows the SROCC score. The SROCC scores for the top six ranked NR-IQA features are shown. Figure 2a shows results obtained when considering the features of a single NR-IQA technique. Figure 2b shows the results when the combination of feature fusion using two NR-IQA techniques at a time is considered. Figure 2c shows the performance when feature fusion is performed with features from three NR-IQA techniques. The performance of the proposed methodology, when features are fused considering features from four NR-IQA techniques is shown in Fig. 2d. The performance when a pool of features from five different NR-IQA techniques are fused is shown in Fig. 2e. Finally, Fig. 2f shows the performance when features from six different NR-IQA techniques are considered. It can be observed

Table 6 Overall performance comparison of the proposed methodology for feature level fusion and feature selection in terms of median values of SROCC, LCC, KCC, RMSE and MAE (mean absolute error) on the LIVEMD and MDID2017 databases

Combination symbol	SROCC	LCC	KCC	RMSE	MAE
BRSQ	0.8804	0.8843	0.6970	2.3690	4.1193
BRSQ-GS	0.8877	0.8914	0.7157	2.3317	4.0722
BRSQ-PSO	0.8424	0.8564	0.6415	2.9272	4.8288
BRSQ-LFS	0.8385	0.8538	0.6387	3.1833	4.9124
BLND2	0.8634	0.8684	0.6779	1.7616	4.4028
BLND2-GS	0.8657	0.8697	0.6726	2.4985	4.2650
BLND2-PSO	0.8448	0.8594	0.6522	2.7375	4.7547
BLND2-LFS	0.8363	0.8503	0.6358	3.2248	4.8955
CQA	0.8325	0.8395	0.6453	2.6400	4.9118
CQA-GS	0.8451	0.8555	0.6487	2.9890	4.6446
CQA-PSO	0.7651	0.7870	0.5510	4.1758	5.7225
CQA-LFS	0.8003	0.8106	0.5974	3.5692	5.1913
DIV	0.9088	0.9148	0.7466	1.9778	4.0368
DIV-GS	**0.9162**	**0.9187**	**0.7538**	**1.8756**	**3.8896**
DIV-PSO	0.8893	0.8905	0.7081	2.3725	4.1224
DIV-LFS	0.8425	0.8581	0.6455	2.9355	4.9605
GLOG	0.8485	0.8616	0.6573	2.7088	4.7315
GLOG-GS	0.8627	0.8683	0.6675	2.5113	4.2921
GLOG-PSO	0.8338	0.8414	0.6364	3.1705	4.8645
GLOG-LFS	0.8098	0.8177	0.6085	3.6511	5.2200
SSEQ	0.7924	0.8018	0.6010	3.5992	5.2895
SSEQ-GS	0.8052	0.8093	0.6034	3.5450	5.0846
SSEQ-PSO	0.7652	0.7799	0.5582	4.5364	5.6096
SSEQ-LFS	0.7652	0.7799	0.5582	4.5964	5.7838
C22	0.9398	0.9420	0.7919	1.7125	3.4976
C22-GS	0.9443	0.9461	0.7982	1.5071	3.3835
C22-PSO	0.9401	0.9426	0.7944	1.6998	3.4842
C22-LFS	0.9051	0.9132	0.7348	3.2906	4.4210
C42	0.9369	0.9396	0.7861	1.8385	3.5247
C42-GS	0.9477	0.9478	0.7983	1.5338	3.3705
C42-PSO	0.9301	0.9338	0.7750	2.0029	3.7289
C42-LFS	0.9153	0.9180	0.7470	2.9372	4.2567
C92	0.9428	0.9461	0.7983	1.8311	3.3992
C92-GS	**0.9515**	**0.9689**	**0.8133**	**1.3937**	**3.2396**
C92-PSO	0.9021	0.9117	0.7325	3.4906	4.5374
C92-LFS	0.9064	0.9139	0.7337	3.2708	4.4071
C12	0.9240	0.9329	0.7858	2.5582	3.8850
C12-GS	0.9316	0.9350	0.7859	1.9414	3.6201
C12-PSO	0.9242	0.9258	0.7685	2.3593	3.8460
C12-LFS	0.8858	0.8987	0.7029	3.8210	4.8042
C52	0.9281	0.9316	0.7740	1.9961	3.7614

Table 6 (continued)

Combination symbol	SROCC	LCC	KCC	RMSE	MAE
C52-GS	0.9359	0.9363	0.7906	1.8735	3.5394
C52-PSO	0.9150	0.9179	0.7477	3.0715	4.2889
C52-LFS	0.8732	0.8893	0.6857	4.1405	5.1203
C62	0.9309	0.9343	0.7744	1.9892	3.7378
C62-GS	0.9323	0.9350	0.7882	1.9485	3.6186
C62-PSO	0.9251	0.9250	0.7708	2.2273	3.8284
C62-LFS	0.8880	0.9077	0.7273	3.6506	4.6053
C123	0.9446	0.9473	0.7993	1.7831	3.5165
C123-GS	0.9484	0.9493	0.8055	1.6621	3.2866
C123-PSO	0.9467	0.9482	0.8032	1.7386	3.3766
C123-LFS	0.9324	0.9351	0.7615	2.4606	3.8215
C33	0.9503	0.9534	0.8122	1.7182	3.2048
C33-GS	**0.9595**	**0.9558**	**0.8184**	**1.4883**	**3.1041**
C33-PSO	0.9130	0.9229	0.7067	3.4283	4.2744
C33-LFS	0.9239	0.9292	0.7313	2.9531	4.1088
C153	0.9441	0.9486	0.7319	1.6931	3.5600
C153-GS	0.9484	0.9503	0.7420	1.5590	3.3493
C153-PSO	0.9452	0.9474	0.8006	1.8301	3.4450
C153-LFS	0.9337	0.9389	0.7676	2.3091	3.7395
C13	0.9447	0.9474	0.8001	1.8261	3.4896
C13-GS	0.9494	0.9499	0.8102	1.6715	3.2812
C13-PSO	0.9431	0.9444	0.7930	1.9063	3.6129
C13-LFS	0.9242	0.9317	0.7518	3.0046	4.0611
C43	0.9403	0.9447	0.7933	1.8679	3.6511
C43-GS	0.9455	0.9462	0.7982	1.8319	3.4579
C43-PSO	0.9341	0.9362	0.7620	2.4563	3.7318
C43-LFS	0.9208	0.9253	0.7246	3.0193	4.1963
C133	0.9427	0.9453	0.7951	1.8674	3.6508
C133-GS	0.9479	0.9484	0.8037	1.7314	3.3532
C133-PSO	0.9440	0.9454	0.7956	1.8674	3.5686
C133-LFS	0.9185	0.9243	0.7212	3.0866	4.2583
C54	0.9456	0.9569	0.8127	1.8007	3.5607
C54-GS	0.9516	0.9545	0.8191	1.6653	3.3447
C54-PSO	0.9492	0.9512	0.8144	1.7548	3.4230
C54-LFS	0.9446	0.9466	0.8095	1.8342	3.6406
C154	0.9475	0.9513	0.8071	1.7815	3.5699
C154-GS	0.9558	0.9584	0.8252	1.4926	3.2351
C154-PSO	0.9515	0.9566	0.8203	1.5984	3.3085
C154-LFS	0.9423	0.9439	0.7960	2.1431	3.6980
C134	0.9521	0.9546	0.8131	1.7345	3.3168
C134-GS	**0.9669**	**0.9592**	**0.8265**	**1.4539**	**3.2021**
C134-PSO	0.9523	0.9575	0.8231	1.5046	3.2685

Table 6 (continued)

Combination symbol	SROCC	LCC	KCC	RMSE	MAE
C134-LFS	0.9365	0.9434	0.7936	2.2044	3.7006
C24	0.9441	0.9443	0.8087	1.7530	3.6552
C24-GS	0.9514	0.9539	0.8188	1.6841	3.3553
C24-PSO	0.9449	0.9485	0.8098	1.8133	3.5828
C24-LFS	0.9260	0.9275	0.7762	2.6679	4.1147
C34	0.9431	0.9495	0.8061	1.8061	3.6927
C34-GS	0.9503	0.9531	0.8155	1.7406	3.3814
C34-PSO	0.9507	0.9534	0.8158	1.7298	3.3781
C34-LFS	0.9332	0.9393	0.7832	2.4370	3.7739
C144	0.9445	0.9472	0.8091	1.8422	3.6200
C144-GS	0.9514	0.9536	0.8179	1.6818	3.3666
C144-PSO	0.9481	0.9507	0.8120	1.7675	3.4448
C144-LFS	0.9361	0.9401	0.7892	2.2649	3.74163
C15	0.9304	0.9366	0.7448	2.0838	3.8442
C15-GS	0.9490	0.9531	0.8072	1.7110	3.4683
C15-PSO	0.9483	0.9529	0.8023	1.7295	3.4843
C15-LFS	0.9390	0.9477	0.7758	1.9011	3.7003
C25	0.9425	0.9493	0.8045	1.8549	3.7479
C25-GS	0.9612	0.9625	0.8337	1.3782	3.3343
C25-PSO	0.9583	0.9578	0.8252	1.5440	3.3887
C25-LFS	0.9531	0.9566	0.8213	1.6335	3.4298
C35	0.9497	0.9531	0.8097	1.8021	3.5012
C35-GS	0.9653	0.9649	0.8414	1.3371	3.3149
C35-PSO	0.9612	0.9630	0.8342	1.4120	3.3458
C35-LFS	0.9515	0.9538	0.8131	1.7576	3.4562
C45	0.9579	0.9614	0.8249	1.6423	3.5114
C45-GS	**0.9715**	**0.9690**	**0.8453**	**1.2646**	**3.2163**
C45-PSO	0.9302	0.9394	0.7621	2.1785	3.8388
C45-LFS	0.9322	0.9399	0.7704	2.1584	3.7884
C55	0.9312	0.9379	0.7454	2.0758	3.8096
C55-GS	0.9466	0.9514	0.7849	1.7976	3.6246
C55-PSO	0.9469	0.9523	0.7911	1.7729	3.5532
C55-LFS	0.9267	0.9366	0.7448	2.9513	3.9399
C65	0.9464	0.9520	0.8072	1.8086	3.5246
C65-GS	0.9597	0.9596	0.8268	1.4356	3.3841
C65-PSO	0.9604	0.9599	0.8299	1.4205	3.3505
C65-LFS	0.9427	0.9489	0.7757	1.9825	3.7465
C16	0.9579	0.9614	0.8249	1.6423	3.5114
C16-GS	**0.9715**	**0.9690**	**0.8453**	**1.2646**	**3.2163**
C16-PSO	0.9302	0.9394	0.7621	2.1785	3.8388
C16-LFS	0.9322	0.9399	0.7704	2.1584	3.7884

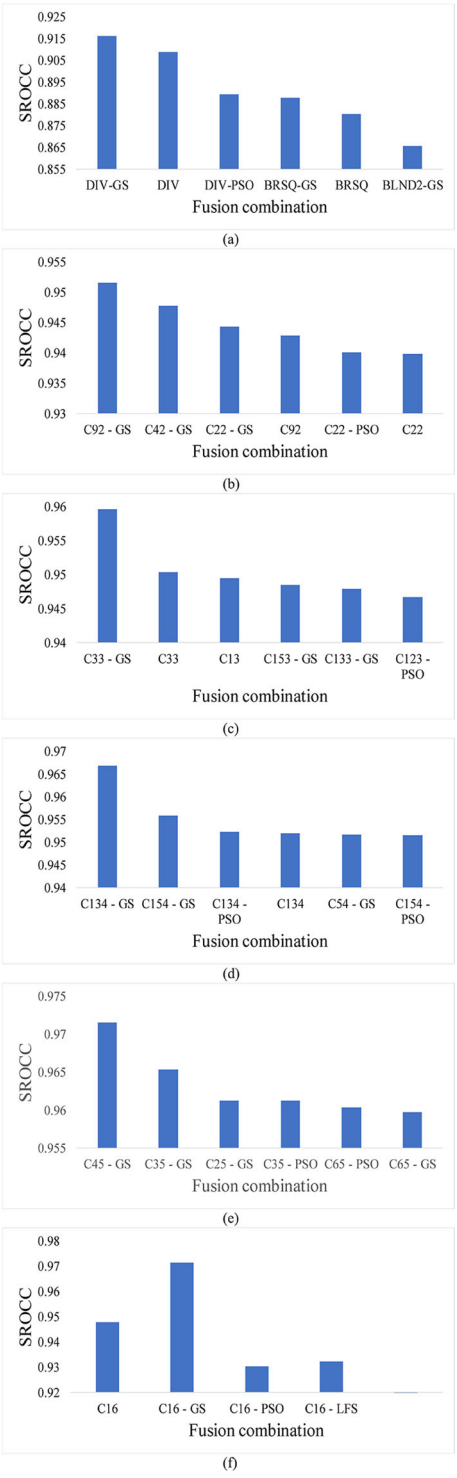

Fig. 2 Overall SROCC score of top performing feature combination with feature selection for the proposed methodology on LIVEMD and MDID2017 databases

that the performance of the proposed methodology improves as the feature fusion from the pool of features is increased from one NR-IQA technique to five NR-IQA technique. The performance remains the same when the pool of features for feature fusion is increased from five NR-IQA techniques to six NR-IQA techniques. It can be observed that DIV-GS has the highest SROCC score of 0.9162 when features from a single NR-IQA technique are considered. C92-GS gives the best results with a SROCC score of 0.9515 when feature fusion is performed from features using two NR-IQA techniques. C33-GS shows the best result of 0.9595 when features are fused from a pool of features from three NR-IQA techniques. C134-GS and C45-GS show the best performance with a SROCC score of 0.9669 and 0.9715 respectively, when the number of NR-IQA techniques considered for feature fusion is four and five respectively. The SROCC score of top-ranked C16-GS remains the same when the features from the number of NR-IQA techniques are increased from five to six.

Figure 3 summarizes the overall performance of the proposed methodology in terms of the LCC score. The x-axis shows the feature vector used and the y-axis shows the LCC score. The SROCC scores for the top six ranked NR-IQA features are shown. The LCC scores for the top six ranked NR-IQA features are shown. Figure 3a shows results obtained when considering the features of a single NR-IQA technique. Figure 3b shows the results when the combination of feature fusion using two NR-IQA techniques at a time is considered. Figure 3c shows the performance when feature fusion is performed with features from three NR-IQA techniques. The performance of the proposed methodology, when features are fused considering features from four NR-IQA techniques is shown in Fig. 3d. The performance when a pool of features from five different NR-IQA techniques are fused is shown in Fig. 3e. Finally, Fig. 3f shows the performance when features from six different NR-IQA techniques are considered. It can be observed that the performance of the proposed methodology improves as the feature fusion from the pool of features is increased from one NR-IQA technique to five NR-IQA technique. The performance remains the same when the pool of features for feature fusion is increased from five NR-IQA techniques to six NR-IQA techniques. It can be observed that DIV-GS has the highest LCC score of 0.9187 when features from a single NR-IQA technique are considered. C92-GS gives the best results with a LCC score of 0.9689 when feature fusion is performed from features using two NR-IQA techniques. C33-GS shows the best result of 0.9558 when features are fused from a pool of features from three NR-IQA techniques. C134-GS and C45-GS show the best performance with a LCC score of 0.9592 and 0.9676 respectively, when the number of NR-IQA techniques considered for feature fusion is four and five respectively. The LCC score of top-ranked C16-GS remains the same when the features from the number of NR-IQA techniques are increased from five to six.

Figure 4 summarizes the overall performance of the proposed methodology in terms of the KCC score. The x-axis shows the feature vector used and the y-axis shows the KCC score. The SROCC scores for the top six ranked NR-IQA features are shown. The KCC scores for the top six ranked NR-IQA features are shown. Figure 4a shows results obtained when considering the features of a single NR-IQA technique. Figure 4b shows the results when the combination of feature fusion using two NR-IQA techniques at a time is considered. Figure 4c shows the performance when feature fusion is performed with features from three NR-IQA techniques. The performance of the proposed methodology, when features are fused considering features from four NR-IQA techniques is shown in Fig. 4d. The performance when a pool of features from five different NR-IQA techniques are fused is shown in Fig. 4e. Finally, Fig. 4f shows the performance when features from six different

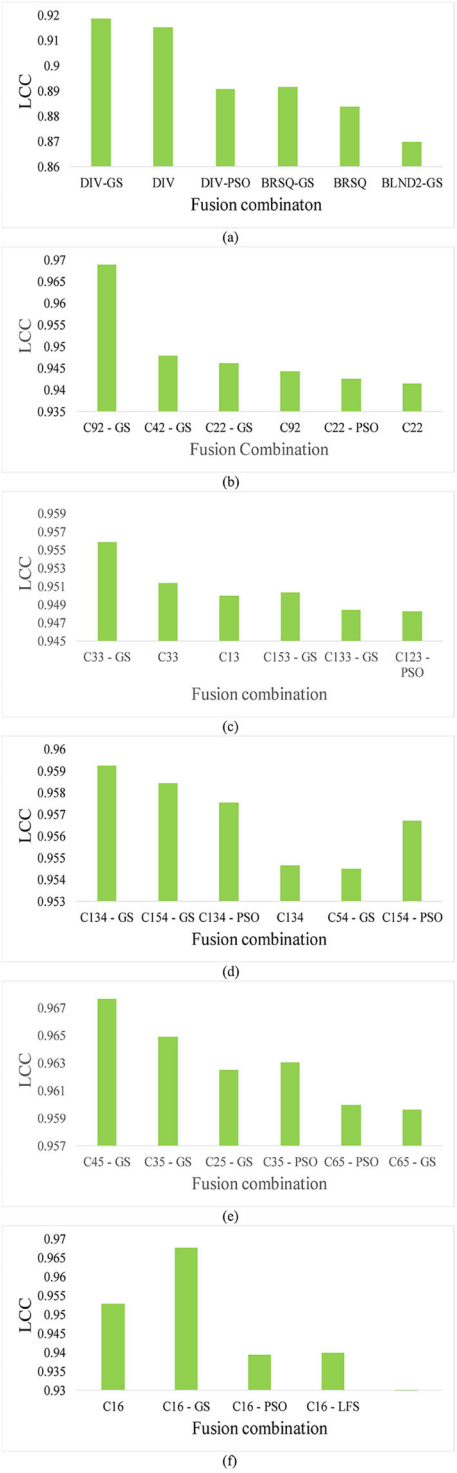

Fig. 3 Overall LCC score of top performing feature combination with feature selection for the proposed methodology on LIVEMD and MDID2017 databases

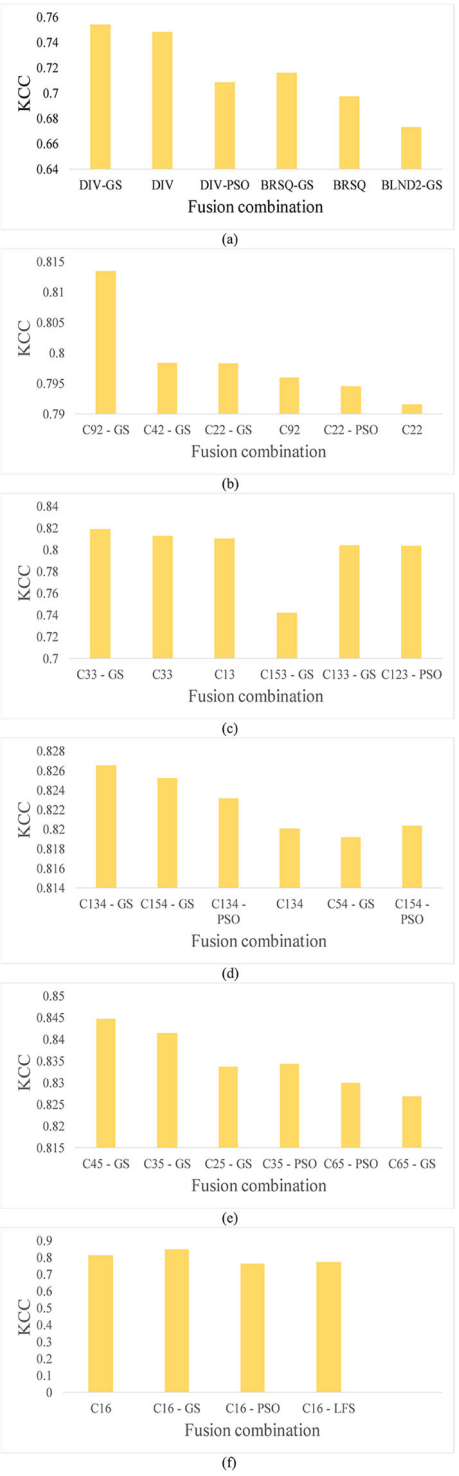

Fig. 4 Overall KCC scores of top performing feature combination with feature selection for the proposed methodology on LIVEMD and MDID2017 databases

NR-IQA techniques are considered. It can be observed that the performance of the proposed methodology improves as the feature fusion from the pool of features is increased from one NR-IQA technique to five NR-IQA technique. The performance remains the same when the pool of features for feature fusion is increased from five NR-IQA techniques to six NR-IQA techniques. It can be observed that DIV-GS has the highest KCC score of 0.7538 when features from a single NR-IQA technique are considered. C92-GS gives the best results with the KCC score of 0.8133 when feature fusion is performed from features using two NR-IQA techniques. C33-GS shows the best result of 0.8184 when features are fused from a pool of features from three NR-IQA techniques. C134-GS and C45-GS show the best performance with a KCC score of 0.8265 and 0.8446 respectively, when the number of NR-IQA techniques considered for feature fusion is four and five respectively. The KCC score of top-ranked C16-GS remains the same when the features from the number of NR-IQA techniques are increased from five to six.

Figure 5 summarizes the overall performance of the proposed methodology in terms of RMSE. The x-axis shows the feature vector used and the y-axis shows the RMSE. The SROCC scores for the top six ranked NR-IQA features are shown. The RMSE for the top six ranked NR-IQA features are shown. Figure 5a shows results obtained when considering the features of a single NR-IQA technique. Figure 5b shows the results when the combination of feature fusion using two NR-IQA techniques at a time is considered. Figure 5c shows the performance when feature fusion is performed with features from three NR-IQA techniques. The performance of the proposed methodology, when features are fused considering features from four NR-IQA techniques is shown in Fig. 5d. The performance when a pool of features from five different NR-IQA techniques are fused is shown in Fig. 5e. Finally, Fig. 5f shows the performance when features from six different NR-IQA techniques are considered. It can be observed that the performance of the proposed methodology improves as the feature fusion from the pool of features is increased from one NR-IQA technique to five NR-IQA technique. The performance remains the same when the pool of features for feature fusion is increased from five NR-IQA techniques to six NR-IQA techniques. It can be observed that DIV-GS has the highest RMSE score of 1.87 when features from a single NR-IQA technique are considered. C92-GS gives the best results with a RMSE score of 1.39 when feature fusion is performed from features using two NR-IQA techniques. C33-GS shows the best result of 1.488 when features are fused from a pool of features from three NR-IQA techniques. C134-GS and C45-GS show the best performance with a RMSE score of 1.454 and 1.31 respectively, when the number of NR-IQA techniques considered for feature fusion is four and five respectively. The RMSE score of top-ranked C16-GS remains the same when the features from the number of NR-IQA techniques are increased from five to six.

Figure 6 shows the performance comparison of the proposed methodology with sixteen state-of-the-art NR-IQA techniques, which include SSIM [42], MS-SSIM [43], FSIM [54], VIF [37], MAD [16], GMSD [46], DESIQUE [52], QAC [45], NIQE [29], ILNIQE [55], BPRI [26], BMPRI [27], GWH-GLBP [18], SISBLIM [10], MUSIQUE [53] and MUSIQUE-II [56]. The x-axis shows the NR-IQA technique and the y-axis shows the SROCC score. The SROCC scores for the top six ranked NR-IQA features are shown. Figure 6a shows the SROCC scores for the NR-IQA techniques on the LIVEMD database. A SROCC score near to 1 represents better performance. It can be observed that the proposed C45-GS and C16-GS perform best with a SROCC score of 0.9691. MISIQUE and MSISQUE-II are ranked second with a SROCC score of 0.8950 and 0.9080 respectively.

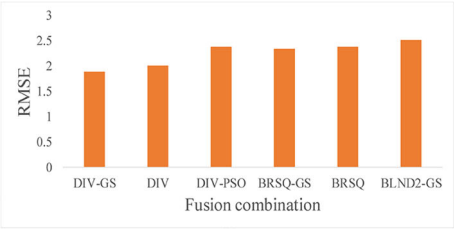

(a)

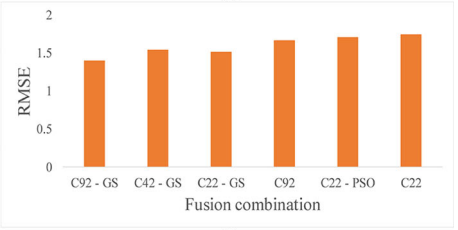

(b)

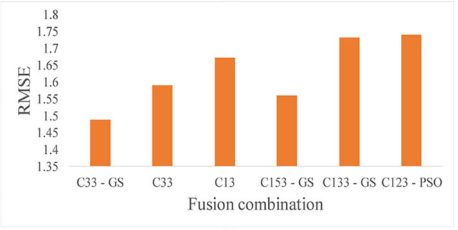

(c)

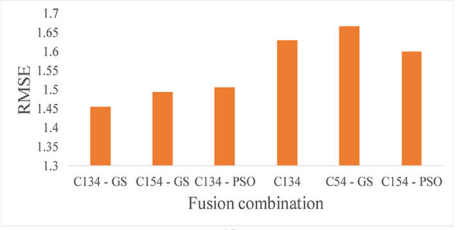

(d)

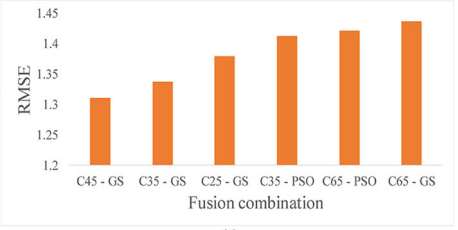

(e)

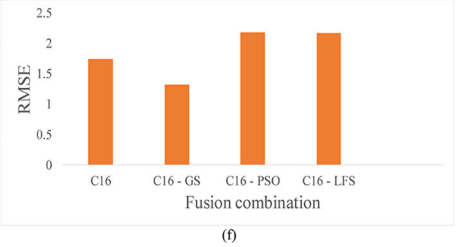

(f)

Fig. 5 Overall RMSE of top performing feature combination with feature selection for the proposed methodology on LIVEMD and MDID2017 databases

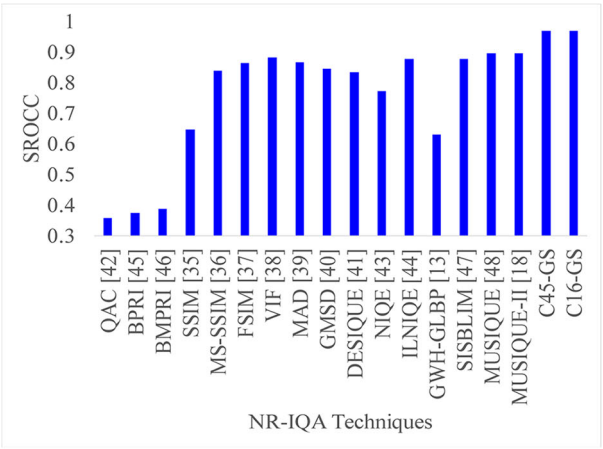

(a)

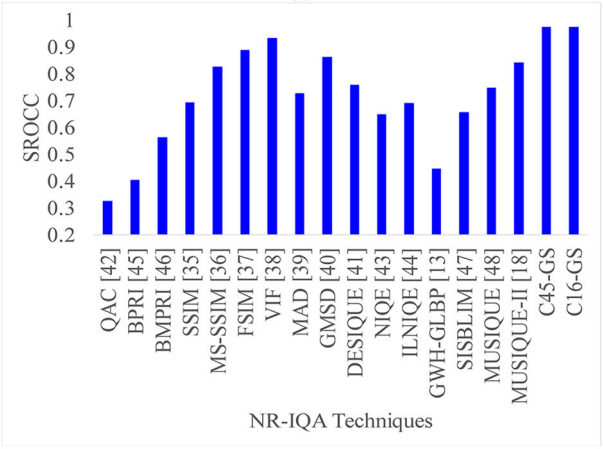

(b)

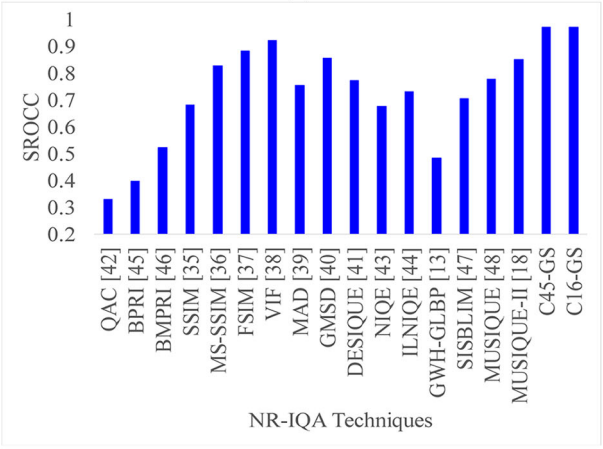

(c)

Fig. 6 Comparison of the proposed methodology with state-of-the-art NR-IQA techniques **a** SROCC over LIVEMD database **b** SROCC over MDID2017 database **c** Overall SROCC over LIVEMD and MDID2017 databases

Figure 6b shows the performance comparison of the proposed methodology with state-of-the-art NR-IQA on the MDID2017 database in terms of the SROCC score. It can be observed that the proposed methodology i.e., C45-GS and C16-GS are ranked top with a SROCC score of 0.9723 each. VIF is ranked second with a SROCC score of 0.9310. Figure 6c shows the overall SROCC score over the LIVEMD and MDID2017 databases. It can be observed that the proposed methodology C45-GS and C16-GS show the best performance with a SROCC score of 0.9716 each, whereas VIF is ranked second with a SROCC score of 0.9202.

Figure 7 shows the performance comparison of the proposed methodology with sixteen state-of-the-art NR-IQA techniques, which include SSIM [42], MS-SSIM [43], FSIM [54], VIF [37], MAD [16], GMSD [46], DESIQUE [52], QAC [45], NIQE [29], ILNIQE [55], BPRI [26], BMPRI [27], GWH-GLBP [18], SISBLIM [10], MUSIQUE [53] and MUSIQUE-II [56]. The x-axis shows the NR-IQA technique and the y-axis shows the LCC score. Figure 7a shows the LCC scores for the NR-IQA techniques on the LIVEMD database. A LCC score near to 1 represents better performance. It can be observed that the proposed C45-GS and C16-GS perform best with a LCC score of 0.9768 each. MISIQUE and MSISQUE-II are ranked second with a LCC score of 0.9090 and 0.9080 respectively. Figure 7b shows the performance comparison of the proposed methodology with state-of-the-art NR-IQA on the MDID2017 database in terms of the LCC score. It can be observed that the proposed methodology i.e., C45-GS and C16-GS are ranked top with a LCC score of 0.9667 each. VIF is ranked second with a LCC score of 0.9370. Figure 7c shows the overall LCC score over the LIVEMD and MDID2017 databases. It can be observed that the proposed methodology C45-GS and C16-GS shows the best performance with a LCC score of 0.9689, whereas VIF is ranked second with a LCC score of 0.9284.

Figure 8 shows the performance comparison of the proposed methodology with sixteen state-of-the-art NR-IQA techniques, which include SSIM [42], MS-SSIM [43], FSIM [54], VIF [37], MAD [16], GMSD [46], DESIQUE [52], QAC [45], NIQE [29], ILNIQE [55], BPRI [26], BMPRI [27], GWH-GLBP [18], SISBLIM [10], MUSIQUE [53] and MUSIQUE-II [56]. The x-axis shows the NR-IQA technique and the y-axis shows the RMSE. Figure 8a shows the performance comparison of the proposed methodology with different NR-IQA in terms of RMSE score on the LIVEMD database, where a RMSE score near to zero shows higher performance. It can be observed that the proposed methodology C45-GS and C16-GS are ranked top with a RMSE of 4.940 each. MUSIQUE-II is ranked second with a RMSE of 7.873. The performance of the proposed methodology on the MDID2017 database in terms of RMSE is shown in Fig. 8b. It can be observed that the proposed methodology i.e., C45-GS and C16-GS show the best performance with a RMSE of 0.1621, furthermore, VIF is ranked second with a RMSE of 0.772. The overall performance comparison of the proposed methodology on the LIVEMD and MDID2017 database in terms of RMSE is shown in Fig. 8c, where the proposed methodology C45-GS and C16-GS are ranked top with a RMSE of 1.2109 each, and VIF is ranked second with a RMSE score of 2.427.

Table 7 shows the overall performance of the proposed methodology on the TID2013, CSIQ, and SIQAD databases. Since the focus of this work is on multi-distorted images therefore, the results of best-performing combinations for the LIVEMD and MDID databases are considered for the TID2013, CSIQ, and SIQAD databases. It can be observed from Table 7 that the for TID2013 database GM-LOG shows the best performance with a SROCC score of 0.6790. The performance improves and shows a SROCC score of 0.6820 when a combination of two NR-IQA techniques is considered. The performance further

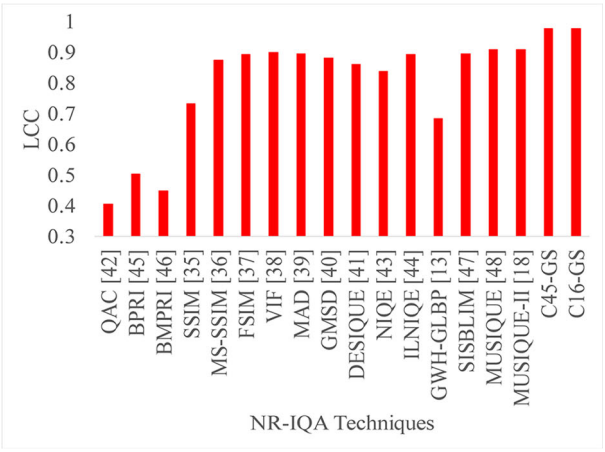

(a)

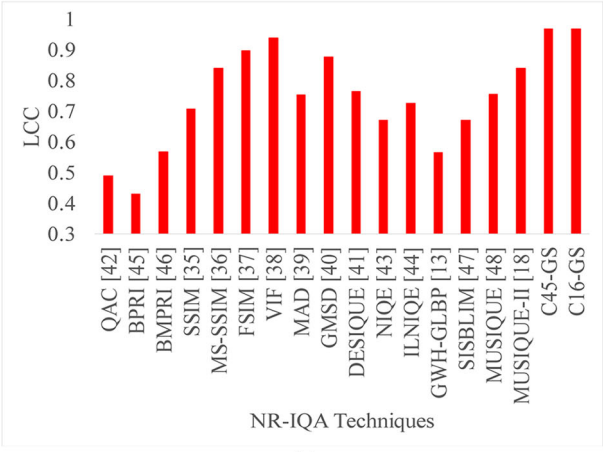

(b)

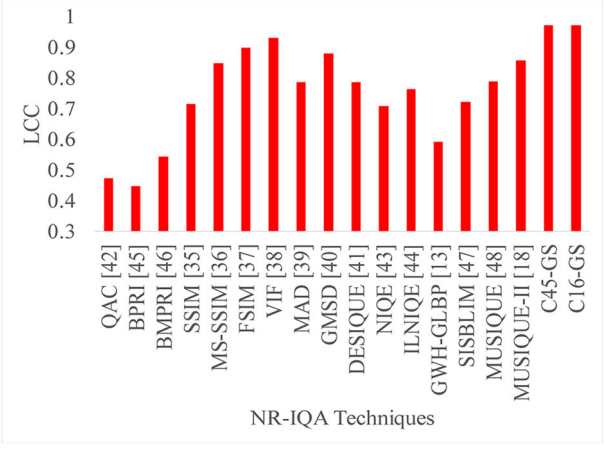

(c)

Fig. 7 Comparison of the proposed methodology with state-of-the-art NR-IQA techniques **a** LCC over LIVEMD database **b** LCC over MDID2017 database **c** Overall LCC on LIVEMD and MDID2017 databases

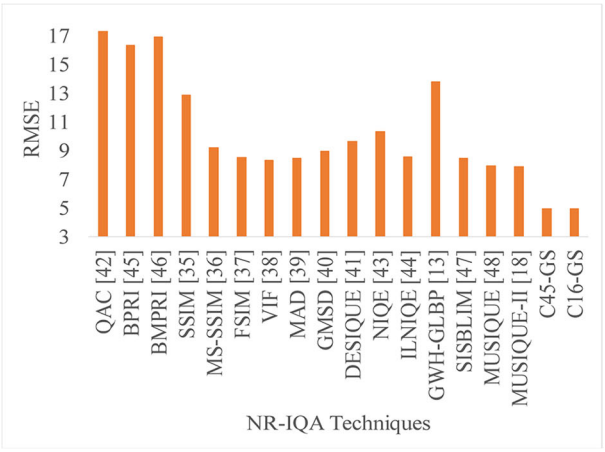

(a)

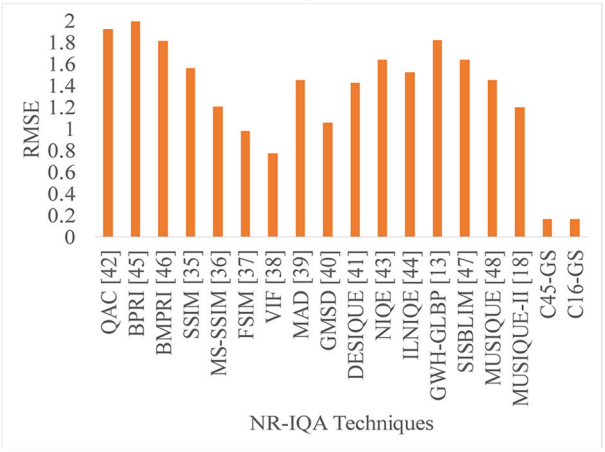

(b)

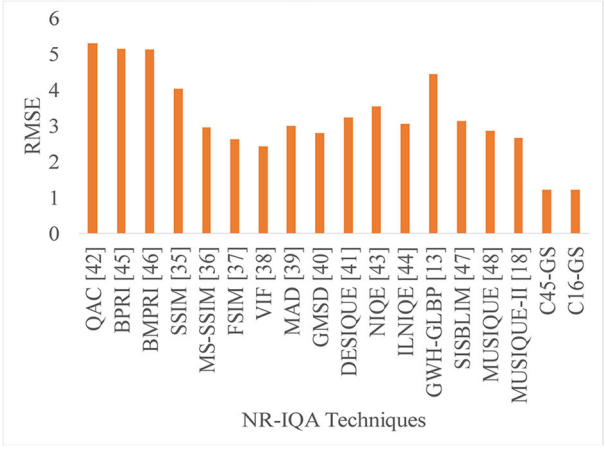

(c)

Fig. 8 Comparison of the proposed methodology with state-of-the-art NR-IQA techniques **a** RMSE over LIVEMD database **b** RMSE over MDID2017 database **c** Overall RMSE on LIVEMD and MDID2017 databases

Table 7 Overall performance of the proposed methodology on the TID2013, CSIQ and SIQAD databases

IQA database	NR-IQA techniques	SROCC	LCC	RMSE
TID2013	BLIINDS-II	0.5360	0.5380	0.6517
	BRISQUE	0.5670	0.5691	0.5669
	DIIVINE	0.5490	0.5540	0.6117
	GM-LOG	0.6790	0.6814	0.4790
	SSEQ	0.5210	0.5217	0.6621
	CurveletQA	0.5517	0.5544	0.6052
	BLND2,CQA	0.6820	0.6870	0.4750
	BLND2,BRSQ,CQA	0.6862	0.6910	0.4715
	BLND2,BRSQ,CQA,SSEQ	0.6870	0.6918	0.4710
	BLND2,BRSQ,CQA,GLOG,SSEQ	0.6892	0.6942	0.4692
	BRQ,BLND2,CQA,DIV,GLOG,SSEQ	0.6892	0.6942	0.4692
CSIQ	BLIINDS-II	0.9003	0.9282	0.1028
	BRISQUE	0.9085	0.9356	0.0980
	DIIVINE	0.8697	0.9010	0.1249
	GM-LOG	0.9243	0.9457	0.0909
	SSEQ	0.8577	0.8614	0.1297
	CurveletQA	0.7891	0.7912	0.2412
	BLND2,CQA	0.9272	0.9473	0.0891
	BLND2,BRSQ,CQA	0.9381	0.9492	0.0851
	BLND2,BRSQ,CQA,SSEQ	0.9412	0.9501	0.0811
	BLND2,BRSQ,CQA,GLOG,SSEQ	0.9452	0.9522	0.0791
	BRQ,BLND2,CQA,DIV,GLOG,SSEQ	0.9452	0.9522	0.0791
SIQAD	BLIINDS-II	0.6813	0.7255	16.312
	BRISQUE	0.7237	0.7708	14.310
	DIIVINE	0.1818	0.2460	32.142
	GM-LOG	0.5821	0.6031	18.210
	SSEQ	0.6921	0.7014	15.910
	CurveletQA	0.7034	0.7122	15.251
	BLND2,CQA	0.7614	0.7742	13.952
	BLND2,BRSQ,CQA	0.7622	0.7750	13.899
	BLND2,BRSQ,CQA,SSEQ	0.7651	0.7762	13.811
	BLND2,BRSQ,CQA,GLOG,SSEQ	0.7682	0.7772	13.752
	BRQ,BLND2,CQA,DIV,GLOG,SSEQ	0.7682	0.7772	13.752

improves, when three NR-IQA techniques are considered and a SROCC score of 0.6862 is achieved. A SROCC score of 0.6870 is obtained when a combination of four NR-IQA techniques is considered. The SROCC score improves to 0.6892 when five or six combinations of NR-IQA techniques are considered. For the CSIQ database GM-LOG shows the best performance with a SROCC score of 0.9243. The performance improves and shows a SROCC score of 0.9272 when a combination of two NR-IQA techniques is considered. The performance further improves, when three NR-IQA techniques are considered and a SROCC

score of 0.9381 is achieved. A SROCC score of 0.9412 is obtained when a combination of four NR-IQA techniques is considered. The SROCC score improves to 0.9452 when five or six combinations of NR-IQA techniques are considered. When the proposed methodology is evaluated on the SIQAD database BRISQUE shows the best performance with a SROCC score of 0.7237. The performance improves and shows a SROCC score of 0.7614 when a combination of two NR-IQA techniques is considered. The performance further improves, when three NR-IQA techniques are considered and a SROCC score of 0.7622 is achieved. A SROCC score of 0.7651 is obtained when a combination of four NR-IQA techniques is considered. The SROCC score improves to 0.7682 when five or six combinations of NR-IQA techniques are considered.

Table 8 shows the overall performance of the proposed methodology on the TID2013, CSIQ, and SIQAD databases when features are selected using the genetic search algorithm. Since the focus of this work is on multi-distorted images therefore, the results of best-performing combinations for the LIVEMD and MDID databases are considered for the TID2013, CSIQ, and SIQAD databases. It can be observed from Table 8 that the for TID2013 database GLOG-GS shows the best performance with a SROCC score of 0.6794. The performance improves and shows a SROCC score of 0.6827 when a combination of two NR-IQA techniques is considered. The performance further improves, when three NR-IQA techniques are considered and a SROCC score of 0.6869 is achieved. A SROCC score of 0.6879 is obtained when a combination of four NR-IQA techniques is considered. The SROCC score improves to 0.6897 when five or six combinations of NR-IQA techniques are considered. For the CSIQ database GLOG-GS shows the best performance with a SROCC score of 0.9250. The performance improves and shows a SROCC score of 0.9282 when a combination of two NR-IQA techniques is considered. The performance further improves, when three NR-IQA techniques are considered and a SROCC score of 0.9389 is achieved. A SROCC score of 0.9422 is obtained when a combination of four NR-IQA techniques is considered. The SROCC score improves to 0.9457 when five or six combinations of NR-IQA techniques are considered. When the proposed methodology is evaluated on the SIQAD database, BRSQ-GS shows the best performance with a SROCC score of 0.7245. The performance improves and shows a SROCC score of 0.7622 when a combination of two NR-IQA techniques is considered. The performance further improves, when three NR-IQA techniques are considered and a SROCC score of 0.7628 is achieved. A SROCC score of 0.7661 is obtained when a combination of four NR-IQA techniques is considered. The SROCC score improves to 0.7695 when five or six combinations of NR-IQA techniques are considered.

Table 9 shows the total number of features for each NR-IQA technique and the number of features selected by each feature selection algorithm. It can be observed that CQA and SSEQ have the lowest number of features i.e., 12 and C16 has the largest number of features i.e., 212. Overall the lowest number of features selected by features selection algorithms is 1 by GS, PSO, and LFS when SSEQ is used. Overall the largest number of features i.e., 84 are selected by GS when the C16 combination is considered. The highest number of features selected by PSO is 71 and LFS is 38 for the C16 combination. The combinations, which are ranked top i.e., C65-GS and C16-GS are 70 and 84 respectively.

Figure 9 shows the features selected using the genetic search algorithm for the six NR-IQA techniques. Genetic search shows the best performance among the feature selection algorithms. Therefore, the analysis of features selected by the genetic search for the best performing combination is presented in Fig. 9a–f. It can be observed that feature numbers 1, 2, 3, 4, 5, 7, 8, 9, 13, 15, and 16 i.e., eleven features out of 24 are selected for BLIINDS-II

Table 8 Overall performance of the proposed methodology using genetic search feature selection algorithm on the TID2013, CSIQ and SIQAD databases

IQA database	NR-IQA techniques	SROCC	LCC	RMSE
TID2013	BLND2-GS	0.5362	0.5386	0.6515
	BRSQ-GS	0.5675	0.5697	0.5661
	DIV-GS	0.5494	0.5547	0.6110
	GLOG-GS	0.6794	0.6818	0.4780
	SSEQ-GS	0.5215	0.5222	0.6615
	CQA-GS	0.5522	0.5551	0.6049
	C92-GS	0.6827	0.6877	0.4745
	C33-GS	0.6869	0.6920	0.4710
	C134-GS	0.6879	0.6926	0.4708
	C45-GS	0.6897	0.6947	0.4688
	C16-GS	0.6897	0.6947	0.4688
CSIQ	BLND2-GS	0.9010	0.9290	0.1022
	BRSQ-GS	0.9093	0.9364	0.0973
	DIV-GS	0.8709	0.9015	0.1242
	GLOG-GS	0.9250	0.9463	0.0900
	SSEQ-GS	0.8583	0.8621	0.1290
	CQA-GS	0.7898	0.7920	0.2402
	C92-GS	0.9282	0.9483	0.0883
	C33-GS	0.9389	0.9502	0.0844
	C134-GS	0.9422	0.9512	0.0802
	C45-GS	0.9457	0.9527	0.0781
	C16-GS	0.9457	0.9527	0.0781
SIQAD	BLND2-GS	0.6820	0.7261	16.306
	BRSQ-GS	0.7245	0.7715	14.302
	DIV-GS	0.1827	0.2467	32.135
	GLOG-GS	0.5830	0.6041	18.201
	SSEQ-GS	0.6933	0.7026	15.900
	CQA-GS	0.7042	0.7133	15.240
	C92-GS	0.7622	0.7752	13.942
	C33-GS	0.7628	0.7760	13.891
	C134-GS	0.7661	0.7772	13.801
	C45-GS	0.7695	0.7785	13.742
	C16-GS	0.7695	0.7785	13.742

NR-IQA. When considering the BRISQUE NR-IQA feature number 2, 3, 5, 6, 7, 9, 10, 13, 14, 15, 17, 18, 20, and 23 i.e., fourteen features out of 36 are selected. For the curveletQA NR-IQA feature numbers 3, 4, and 7 i.e., three features out of 12 are selected. The DIIVINE NR-IQA has a total of 88 features, out of which 44 features are selected i.e., feature numbers 2, 3, 5, 6, 14, 15, 16, 17, 18, 21, 25, 26, 27, 28, 29, 30, 31, 32, 33, 34, 35, 36, 37, 38, 39, 40, 41, 42, 43, 47, 52, 57, 62, 67, 72, 74, 77, 78, 81, 82, 83, 84, 85 and 86. GM-LOG extracts

Table 9 Number of features selected by feature selection algorithms for the proposed methodology

NR-IQA techniques	All	GS	PSO	LFS
BRISQUE	36	14	8	4
BLIINDS-II	24	11	11	5
CQA	12	3	3	5
DIIVINE	88	44	36	17
GM-LOG	40	11	12	6
SSEQ	12	1	1	1
BRSQ,CQA	48	17	11	9
BRSQ,DIV	124	58	44	21
BRSQ,GLOG	76	25	20	10
BRSQ,SSEQ	48	15	9	5
BLND2,BRSQ	60	25	19	9
CQA,DIV	100	47	39	22
CQA,GLOG	52	14	15	11
CQA,SSEQ	24	4	4	6
BLND2,CQA	36	14	14	10
DIV,GLOG	128	55	48	23
DIV,SSEQ	90	45	45	18
BLND2,DIV	112	55	47	22
BLND2,GLOG	64	22	23	11
GLOG,SSEQ	52	12	13	7
BLND2,SSEQ	36	12	12	6
BRSQ,CQA,DIV	136	61	47	26
BRSQ,CQA,GLOG	136	28	23	15
BLND2,BRSQ,CQA	72	28	22	14
BRSQ,CQA,SSEQ	60	18	12	10
CQA,DIV,GLOG	140	58	51	28
BLND2,CQA,DIV	124	58	51	27
CQA,DIV,SSEQ	112	48	40	23
BLND2,DIV,GLOG	152	66	59	28
DIV,GLOG,SSEQ	140	56	59	24
BLND2,GLOG,SSEQ	76	23	24	12
BLND2,DIV,SSEQ	124	56	48	23
BLND2,BRSQ,DIV	148	69	55	26
BRSQ,DIV,SSEQ	136	59	45	22
BRSQ,DIV,GLOG	164	69	56	27
BRSQ,CQA,DIV,GLOG	176	72	59	32
BLND2,BRSQ,CQA,DIV	160	72	58	31
BRSQ,CQA,DIV,SSEQ	148	62	48	27
BLND2,DIV,GLOG,SSEQ	164	67	60	29
BLND2,CQA,DIV,SSEQ	136	59	51	28
BLND2,CQA,DIV,GLOG	164	69	62	33
CQA,DIV,GLOG,SSEQ	152	59	52	29
BLND2,BRSQ,DIV,SSEQ	160	70	56	27

Table 9 (continued)

NR-IQA techniques	All	GS	PSO	LFS
BLND2,BRSQ,DIV,GLOG	188	80	67	32
BRSQ,DIV,GLOG,SSEQ	176	70	57	28
BLND2,BRSQ,CQA,DIV,GLOG	200	83	70	37
BRSQ,CQA,DIV,GLOG,SSEQ	188	73	60	33
BLND2,BRSQ,CQA,DIV,SSEQ	172	73	59	32
BLND2,BRSQ,CQA,GLOG,SSEQ	124	40	35	21
BLND2,BRSQ,DIV,GLOG,SSEQ	200	81	68	33
BLND2,CQA,DIV,GLOG,SSEQ	176	70	63	34
BLND2,BRSQ,CQA,DIV,GLOG,SSEQ	212	84	71	38

a total of 40 features and feature numbers 13, 15, 17, 18, 19, 20, 28, 29, 31, 32, and 35 i.e., eleven features are selected. Only one feature i.e., feature number 3 is selected for the SSEQ NR-IQA.

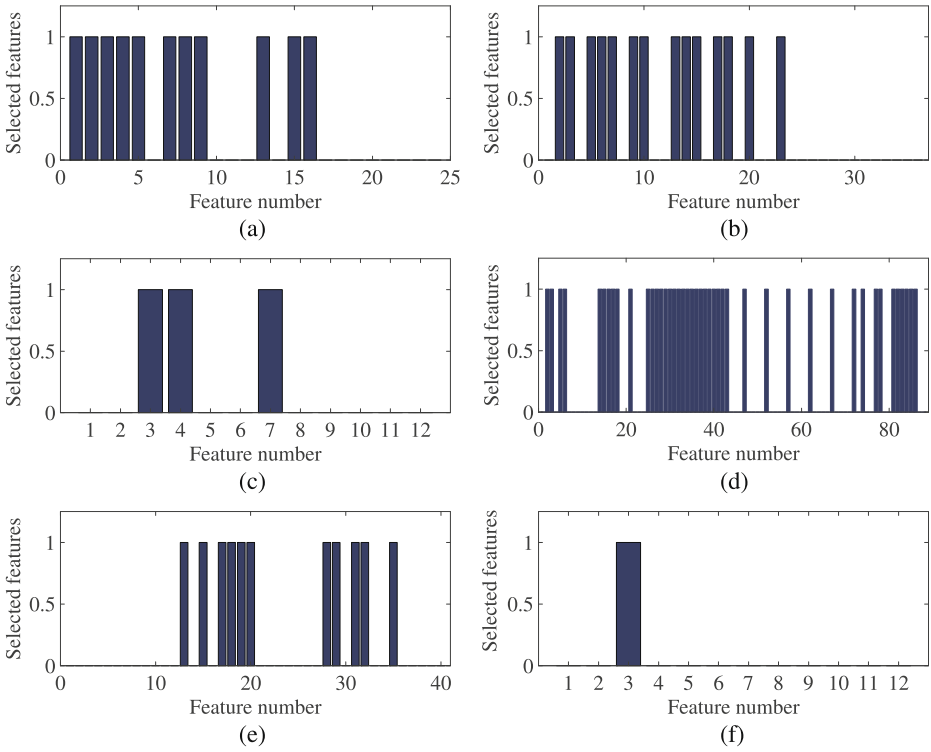

Fig. 9 Features selected using genetic search algorithm for each NR-IQA **a** BLIINDS-II, **b** BRISQUE, **c** curveletQA, **d** DIIVINE **e** GM-LOG, **f** SSEQ

4 Conclusion and future works

The evolution of technology and the availability of mobile devices have made multimedia a daily part of our lives. Images taken by these devices may be affected by multiple distortions. Therefore, the image quality assessment of multiply distorted images has gained importance. But it is a challenging task, due to the presence of more than one type of distortions in an image. In this work, features are extracted from different domains using six different NR-IQA techniques. Feature level fusion is performed using all combinations of features from different domains, where these features are used to assess the quality of images. The fused features from different domains may be redundant and irrelevant. Therefore, feature selection algorithms are used to select optimum features for IQA to multiply distorted images. The most common evaluation parameters used to evaluate the performance of NR-IQA techniques are SROCC, LCC, KCC, and RMSE. SROCC, LCC, and KCC measure the correlation, whereas RMSE measures the error between the subjective and predicted quality scores. The features extracted in different domains carry different statistical properties that can help in assessing the extent of degradation in the image. The features extracted in the DCT domain show symmetric distribution that can be modeled using a GGD, which changes proportionally to the type and extent of distortion in an image. The scalar energy-based features extracted in the curvelet domain have rich information of orientation and scale and curvelet transform can change its window size in the extraction of scale information without any information regarding the scaling factor. The statistics of features extracted using curvelet transform changes with distortion type and extent of distortion in the image. The normalized luminance coefficients for natural undistorted images extracted in the spatial domain follow a Gaussian distribution, which does not hold for the distorted images. The spectral features extracted using spectral entropy measures the statistical information in the image, which is disrupted in the presence of distortion. The image local contrast features extracted in the spatial domain that includes gradient and Laplacian of Gaussian contains important information about the image perceptual quality. The wavelet coefficients extracted in multiscale decomposition mimics the spatial decomposition that occurs in the V1 area of the primary visual cortex. It is observed that the performance to predict multiple-distorted image quality score is improved by fusing features from different domains. The best performance is obtained when feature level fusion is performed using features from spatial, spectral, DCT, wavelet, and curvelet domains. Furthermore, it is also observed that applying a feature selection algorithm on fused features helps in selecting the optimal features for IQA of multiply distorted images. The genetic search algorithm showed the best performance to predict the multiple-distorted image quality score when combined with feature level fusion. In the future, we intend to propose new feature selection algorithms specifically designed for multiple distorted NR-IQA to further improve the performance with evaluation parameters for the selection of features as SROCC, LCC, KCC, and RMSE.

References

1. Chen Y, Wang J, Chen X, Zhu M, Yang K, Wang Z, Xia R (2019) Single-image super-resolution algorithm based on structural self-similarity and deformation block features. IEEE Access 7:58791–58801
2. Chen Y, Wang J, Liu S, Chen X, Xiong J, Xie J, Yang K (2019) Multiscale fast correlation filtering tracking algorithm based on a feature fusion model. Concurrency and Computation: Practice and Experience: e5533

3. Chen Y, Wang J, Xia R, Zhang Q, Cao Z, Yang K (2019) The visual object tracking algorithm research based on adaptive combination kernel. Journal of Ambient Intelligence and Humanized Computing 10(12):4855–4867
4. Chen Y, Xiong J, Xu W, Zuo J (2019) A novel online incremental and decremental learning algorithm based on variable support vector machine. Clust Comput 22(3):7435–7445
5. Chen Y, Xu W, Zuo J, Yang K (2019) The fire recognition algorithm using dynamic feature fusion and iv-svm classifier. Clust Comput 22(3):7665–7675
6. Chen Y, Liu L, Tao J, Xia R, Zhang Q, Yang K, Xiong J, Chen X (2020) The improved image inpainting algorithm via encoder and similarity constraint. Vis Comput: 1–15
7. Chen Y, Tao J, Liu L, Xiong J, Xia R, Xie J, Zhang Q, Yang K (2020) Research of improving semantic image segmentation based on a feature fusion model. Journal of Ambient Intelligence and Humanized Computing
8. Chen Y, Tao J, Zhang Q, Yang K, Chen X, Xiong J, Xia R, Xie J (2020) Saliency detection via the improved hierarchical principal component analysis method. Wireless Communications and Mobile Computing
9. Dai T, Gu K, Niu L, Zhang Y-B, Lu W, Xia S-T (2018) Referenceless quality metric of multiply-distorted images based on structural degradation. Neurocomputing 290:185–195
10. Gu K, Zhai G, Yang X, Zhang W (2014) Hybrid no-reference quality metric for singly and multiply distorted images. IEEE Trans Broadcast 60(3):555–567
11. Gutlein M, Frank E, Hall M, Karwath A (2009) Large-scale attribute selection using wrappers. In: IEEE Symposium on computational intelligence and data mining, 2009. CIDM'09. IEEE, pp 332–339
12. Jayaraman D, Mittal A, Moorthy AK, Bovik AC (2012) Objective quality assessment of multiply distorted images. In: 2012 conference record of the forty sixth asilomar conference on signals, systems and computers, ASILOMAR. IEEE, pp 1693–1697
13. Jiang Q, Shao F, Gao W, Chen Z, Jiang G, Ho Y-S (2018) Unified no-reference quality assessment of singly and multiply distorted stereoscopic images. IEEE Trans Image Process 28(4):1866–1881
14. Kalatehjari E, Yaghmaee F (2018) A new reduced-reference image quality assessment based on the svd signal projection. Multimedia Tools and Applications 77(19):25053–25076
15. Kennedy J. (2011) Particle swarm optimization. In: Encyclopedia of machine learning. Springer, Berlin, pp 760–766
16. Larson EC, Chandler DM (2010) Most apparent distortion: full-reference image quality assessment and the role of strategy. Journal of Electronic Imaging 19(1):011006
17. Lay DC (2006) Linear algebra and its applications third edition update, University of Maryland, College Park
18. Li Q, Lin W, Fang Y (2016) No-reference quality assessment for multiply-distorted images in gradient domain. IEEE Signal Processing Letters 23(4):541–545
19. Li C, Li Y, Yuan Y, Wu X, Sang Q (2018) Quaternion wavelet transform based full reference image quality assessment for multiply distorted images. PloS one 13(6)
20. Li C, Zhang Y, Wu X, Zheng Y (2018) A multi-scale learning local phase and amplitude blind image quality assessment for multiply distorted images. IEEE Access 6:64577–64586
21. Liao X, Li K, Yin J (2017) Separable data hiding in encrypted image based on compressive sensing and discrete fourier transform. Multimedia Tools and Applications 76(20):20739–20753
22. Liu L, Dong H, Huang H, Bovik AC (2014) No-reference image quality assessment in curvelet domain. Signal Processing: Image Communication 29(4):494–505
23. Liu L, Liu B, Huang H, Bovik AC (2014) No-reference image quality assessment based on spatial and spectral entropies. Signal Processing: Image Communication 29(8):856–863
24. Luo Y, Qin J, Xiang X, Tan Y, Liu Q, Xiang L (2020) Coverless real-time image information hiding based on image block matching and dense convolutional network. J Real-Time Image Proc 17(1):125–135
25. Miao X, Chu H, Liu H, Yang Y, Li X (2019) Quality assessment of images with multiple distortions based on phase congruency and gradient magnitude. Signal Processing: Image Communication 79:54–62
26. Min X, Gu K, Zhai G, Liu J, Yang X, Chen CW (2017) Blind quality assessment based on pseudo-reference image. IEEE Transactions on Multimedia 20(8):2049–2062
27. Min X, Zhai G, Gu K, Liu Y, Yang X (2018) Blind image quality estimation via distortion aggravation. IEEE Trans Broadcast 64(2):508–517
28. Mittal A, Moorthy AK, Bovik AC (2012) No-reference image quality assessment in the spatial domain. IEEE Trans Image Process 21(12):4695–4708
29. Mittal A, Soundararajan R, Bovik AC (2012) Making a completely blind image quality analyzer. IEEE Signal Processing Letters 20(3):209–212

30. Moorthy AK, Bovik AC (2011) Blind image quality assessment: from natural scene statistics to perceptual quality. IEEE Trans Image Process 20(12):3350–3364
31. Nizami IF, Majid M, Afzal H, Khurshid K (2018) Impact of feature selection algorithms on blind image quality assessment. Arab J Sci Eng 43(8):4057–4070
32. Nizami IF, Majid M, Khurshid K (2018) New feature selection algorithms for no-reference image quality assessment. Appl Intell 48(10):3482–3501
33. Nizami IF, Majid M, Manzoor W, Khurshid K, Jeon B (2019) Distortion-specific feature selection algorithm for universal blind image quality assessment. EURASIP Journal on Image and Video Processing 2019(1):19
34. Nizami IF, Majid M, ur Rehman M, Anwar SM, Nasim A, Khurshid K (2020) No-reference image quality assessment using bag-of-features with feature selection. Multimedia Tools and Applications 79(11):1–26
35. Ponomarenko N, Jin L, Ieremeiev O, Lukin V, Egiazarian K, Astola J, Vozel B, Chehdi K, Carli M, Battisti F, et al. (2015) Image database tid2013: peculiarities, results and perspectives. Signal Processing: Image Communication 30:57–77
36. Saad MA, Bovik AC, Charrier C (2012) Blind image quality assessment: a natural scene statistics approach in the dct domain. IEEE Trans Image Process 21(8):3339–3352
37. Sheikh HR, Bovik AC (2006) Image information and visual quality. IEEE Trans Image Process 15(2):430–444
38. Siedlecki W, Sklansky J (1989) A note on genetic algorithms for large-scale feature selection. Pattern Recogn Lett 10(5):335–347
39. Sun W, Liao Q, Xue J-H, Zhou F (2018) Spsim: a superpixel-based similarity index for full-reference image quality assessment. IEEE Trans Image Process 27(9):4232–4244
40. Sun L, Wu F, Zhan T, Liu W, Wang J, Jeon B (2020) Weighted nonlocal low-rank tensor decomposition method for sparse unmixing of hyperspectral images. IEEE Journal of Selected Topics in Applied Earth Observations and Remote Sensing 13:1174–1188
41. Sun W, Zhou F, Liao Q (2017) Mdid: a multiply distorted image database for image quality assessment. Pattern Recogn 61:153–168
42. Wang Z, Bovik AC, Sheikh HR, Simoncelli EP (2004) Image quality assessment: from error visibility to structural similarity. IEEE Trans Image Process 13(4):600–612
43. Wang Z, Simoncelli EP, Bovik AC (2003) Multiscale structural similarity for image quality assessment. In: Conference record of the thirty-seventh asilomar conference on signals, systems and computers, 2004, vol 2. IEEE, pp 1398–1402
44. Xue W, Mou X, Zhang L, Bovik AC, Feng X (2014) Blind image quality assessment using joint statistics of gradient magnitude and laplacian features. IEEE Trans Image Process 23(11):4850–4862
45. Xue W, Zhang L, Mou X (2013) Learning without human scores for blind image quality assessment. In: Proceedings of the IEEE conference on computer vision and pattern recognition, pp 995–1002
46. Xue W, Zhang L, Mou X, Bovik AC (2013) Gradient magnitude similarity deviation: a highly efficient perceptual image quality index. IEEE Trans Image Process 23(2):684–695
47. Yang H, Fang Y, Lin W (2015) Perceptual quality assessment of screen content images. IEEE Trans Image Process 24(11):4408–4421
48. Yin X, Zhang M, Wang L, Liu Y (2020) Interface debonding performance of precast segmental nanomaterials based concrete (psnbc) beams. Materials Express 10(8):1317–1327
49. Yu F, Liu L, He B, Huang Y, Shi C, Cai S, Song Y, Du S, Wan Q (2019) Analysis and fpga realization of a novel 5d hyperchaotic four-wing memristive system, active control synchronization, and secure communication application. Complexity
50. Yu F, Liu L, Xiao L, Li K, Cai S (2019) A robust and fixed-time zeroing neural dynamics for computing time-variant nonlinear equation using a novel nonlinear activation function. Neurocomputing 350:108–116
51. Yue G, Hou C, Gu K, Ling N, Li B (2018) Analysis of structural characteristics for quality assessment of multiply distorted images. IEEE Transactions on Multimedia 20(10):2722–2732
52. Zhang Y, Chandler DM (2013) No-reference image quality assessment based on log-derivative statistics of natural scenes. Journal of Electronic Imaging 22(4):043025
53. Zhang Y, Chandler DM (2018) Opinion-unaware blind quality assessment of multiply and singly distorted images via distortion parameter estimation. IEEE Trans Image Process 27(11):5433–5448
54. Zhang L, Zhang L, Mou X, Zhang D (2011) Fsim: a feature similarity index for image quality assessment. IEEE Trans Image Process 20(8):2378–2386
55. Zhang L, Zhang L, Bovik AC (2015) A feature-enriched completely blind image quality evaluator. IEEE Trans Image Process 24(8):2579–2591

56. Zhang Y, Mou X, Chandler DM (2019) Learning no-reference quality assessment of multiply and singly distorted images with big data. IEEE Transactions on Image Processing
57. Zhou L, Zhang T, Tian Y, Huang H (2020) Fraction-order total variation image blind restoration based on self-similarity features. IEEE Access 8:30436–30444
58. Zhu W, Zhai G, Min X, Hu M, Liu J, Guo G, Yang X (2019) Multi-channel decomposition in tandem with free-energy principle for reduced-reference image quality assessment. IEEE Transactions on Multimedia 21(9):2334–2346

Affiliations

Imran Fareed Nizami[1] · Mehreen Akhtar[2] · Asad Waqar[1] · Amer Bilal Mann[3] · Muhammad Majid[2]

Muhammad Majid
m.majid@uettaxila.edu.pk

[1] Department of Electrical Engineering, Bahria University, Islamabad, Pakistan

[2] Department of Computer Engineering, University of Engineering and Technology Taxila, Punjab, Pakistan

[3] Department of Mathematical Sciences, Federal Urdu University of Arts, Science and Technology, Islamabad, Pakistan